Palaeogeography, Palaeoclimatology, Palaeoecology 512 (2018) 6–22

Contents lists available at ScienceDirect

Palaeogeography, Palaeoclimatology, Palaeoecology

journal homepage: www.elsevier.com/locate/palaeo

Qaidam Basin paleosols reflect climate and weathering intensity on the northeastern Tibetan Plateau during the Early Eocene Climatic Optimum

Bowen Song[a,b,*], Kexin Zhang[a,b,c], Li Zhang[a], Junliang Ji[b,c], Hanlie Hong[b,c], Yi Wei[d], Yadong Xu[b,c], Thomas J. Algeo[b,e,f], Chaowen Wang[g,**]

[a] Institute of Geological Survey, China University of Geosciences, Wuhan 430074, China
[b] State Key Laboratory of Biogeology and Environmental Geology, China University of Geosciences, Wuhan 430074, China
[c] Faculty of Earth Sciences, China University of Geosciences, Wuhan 430074, China
[d] Safety Engineering College, North China Institute of Science & Technology, Langfang 065210, China
[e] State Key Laboratory of Geological Processes and Mineral Resources, China University of Geosciences, Wuhan 430074, China
[f] Department of Geology, University of Cincinnati, Cincinnati, OH 45221-0013, USA
[g] Gemological Institute, China University of Geosciences, Wuhan 430074, China

ARTICLE INFO

Keywords:
Paleoclimate
Smectite
Chemical weathering
Paleoelevation
Stable isotope

ABSTRACT

As an important geological archive, paleosols have been widely used in reconstruction of paleoenvironmental and paleoclimatic conditions. In this study, we undertook detailed analyses of the clay mineralogy and carbon and oxygen isotopic compositions of pedogenic carbonates in a series of 13 paleosol horizons within a fluvial section of the Eocene (~52–44 Ma) Lulehe Formation in the Qaidam Basin. Pedogenic smectite and illite/smectite (I/S) mixed-layer minerals are the predominant clay minerals in the paleosols, suggesting that the early Eocene paleoclimate of the Qaidam Basin was strongly seasonal with warm-wet summers. The high levels of pedogenic smectite production and high atmospheric pCO_2 reconstructed from soil carbonate nodule $\delta^{13}C$ (mean $-7.1 \pm 0.8‰$) are consistent with elevated temperatures during the Early Eocene Climatic Optimum (EECO). Coeval paleosol carbonate nodules yield estimated paleo-surface water compositions ($\delta^{18}O_{psw}$) of $-7.9‰$ to $-6.0‰$ (VSMOW), which are significantly higher than the $\delta^{18}O$ value of modern summer precipitation in the Qaidam Basin. The estimated temperature difference (~5.0 °C cooling) implies uplift of the study area by nearly 1000 m to its current average elevation of ~3000 m above sea level. This paleoelevation estimate agrees with modern meteoric water isotopes of Global Network of Isotopes in Precipitation (GNIP) sites in Asia in the same elevation range.

1. Introduction

Paleosols preserved in continental sedimentary successions archive information about paleoenvironmental and paleoclimatic changes (Sheldon and Tabor, 2009). Paleosols have been widely used to reconstruct soil-forming climate factors such as precipitation amount, temperature, and atmospheric pCO_2 level in ancient sedimentary systems (Quade et al., 1989; Cerling and Quade, 1993; Sheldon et al., 2002; Retallack, 2001a, 2001b, 2005, 2007; Breecker et al., 2009; Singh et al., 2012).

The rise of the Tibetan Plateau during the Cenozoic led to formation of multiple intracontinental basins containing thick sedimentary successions that can be used to study its uplift history and regional tectonic-climatic coupling (Dettman et al., 2003; Fang et al., 2003, 2007; Dupont-Nivet et al., 2007, 2008; Zhang et al., 2008; Kent-Corson et al., 2009; Xiao et al., 2010; Miao et al., 2011; Abels et al., 2011; Hough et al., 2011; Zhuang et al., 2011a; Sun et al., 2014; Ding et al., 2014). Located on the northeastern Tibetan Plateau, the Qaidam Basin accumulated a thick stratal succession (up to 15 km) spanning the early Eocene to Quaternary, making it an excellent candidate for reconstruction of Cenozoic paleoenvironmental records. Although Cenozoic paleoenvironments of the Qaidam Basin have been intensively investigated (e.g., Wang et al., 1999; Kent-Corson et al., 2009; Miao et al., 2011; Zhuang et al., 2011a; Liu et al., 2014; Jian et al., 2014; Song et al., 2014; Cheng and Yang, 2016; Song et al., 2017), lower Eocene fluvial-paleosol systems have received little attention to date. In this paper, we present new stable isotope data and clay-mineral compositions for 13 paleosols of the Lulehe Formation in order to

* Correspondence to: B. Song, Institute of Geological Survey, China University of Geosciences, Wuhan 430074, China.
** Corresponding author.
E-mail addresses: bwsong1985@cug.edu.cn (B. Song), cwwang_cug@aliyun.com (C. Wang).

https://doi.org/10.1016/j.palaeo.2018.03.027
Received 24 August 2017; Received in revised form 18 March 2018; Accepted 23 March 2018
Available online 26 March 2018
0031-0182/ © 2018 Elsevier B.V. All rights reserved.

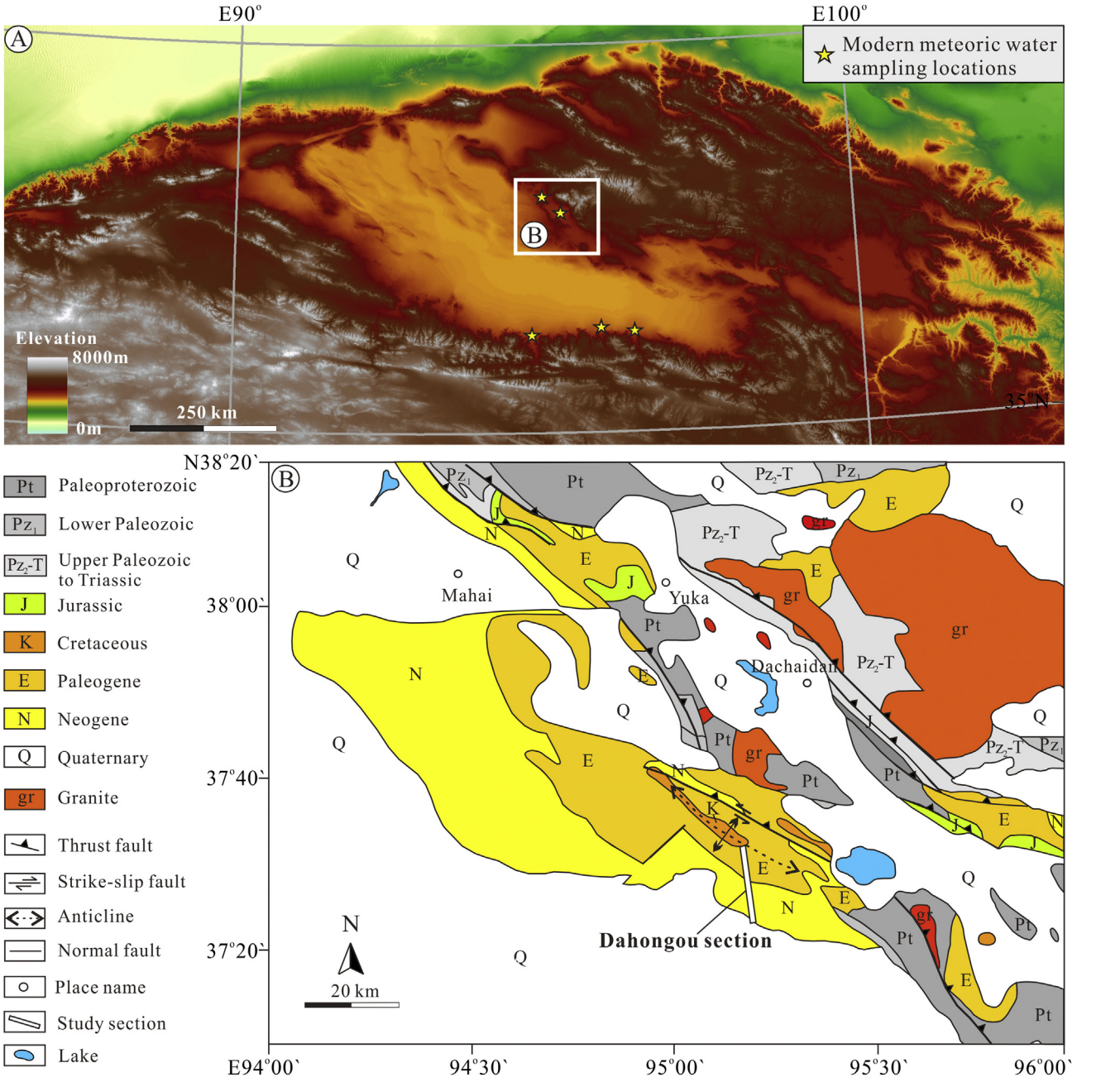

Fig. 1. (A). Geographic location of the Qaidam Basin in the northern Tibetan Plateau. The map shows modern meteoric water sampling locations. Inset represents the study area. (B) Geological map of the study area, showing location of the studied section.

reconstruct early Eocene paleoenvironmental conditions in the Qaidam Basin and improve our understanding of the paleotopography of the contemporaneous northeastern Tibetan Plateau.

2. Geological setting and stratigraphy

2.1. Study area and section

The Qaidam Basin, with an average elevation of ~3000 m, is the largest intermontane basin within the northeastern Tibetan Plateau (Liu et al., 1998; Metivier et al., 1998) (Fig. 1A). The basin is bounded by three large mountain ranges: the Qilian Mountains to the north, the Kunlun-Qimantagh Mountains to the south, and the Altyn Mountains to the west (QBGMR, 1991; Xia et al., 2001; Rieser et al., 2005; Bush et al., 2016). The present-day Qaidam Basin has an arid desert climate with a mean annual precipitation (MAP) of < 100 mm and potential evaporation > 2000 mm (Wang et al., 1999). Cenozoic deposition in the Qaidam Basin was initiated in the early Eocene, synchronous with the India-Asia collision, yielding basin fills up to 15 km in thickness (Huang et al., 1996). The Cenozoic succession of the Qaidam Basin consists of seven formations whose ages have been constrained based on basin-wide lithostratigraphic, paleontologic, and magnetostratigraphic frameworks (from oldest to youngest): the Lulehe (lower–middle Eocene), Xia Ganchaigou (upper Eocene–lower Oligocene), Shang Ganchaigou (upper Oligocene–lower Miocene), Xia Youshashan (lower Miocene–middle Miocene), Shang Youshashan (middle–upper Miocene), Shizigou (upper Miocene–Pliocene), and Qigequan (Pliocene–Pleistocene) Formations (Yang et al., 1992; Sun et al., 2005; Fang et al., 2007; Wang et al., 2007; Lu and Xiong, 2009; Ke et al., 2013; Chang et al., 2015; Ji et al., 2017).

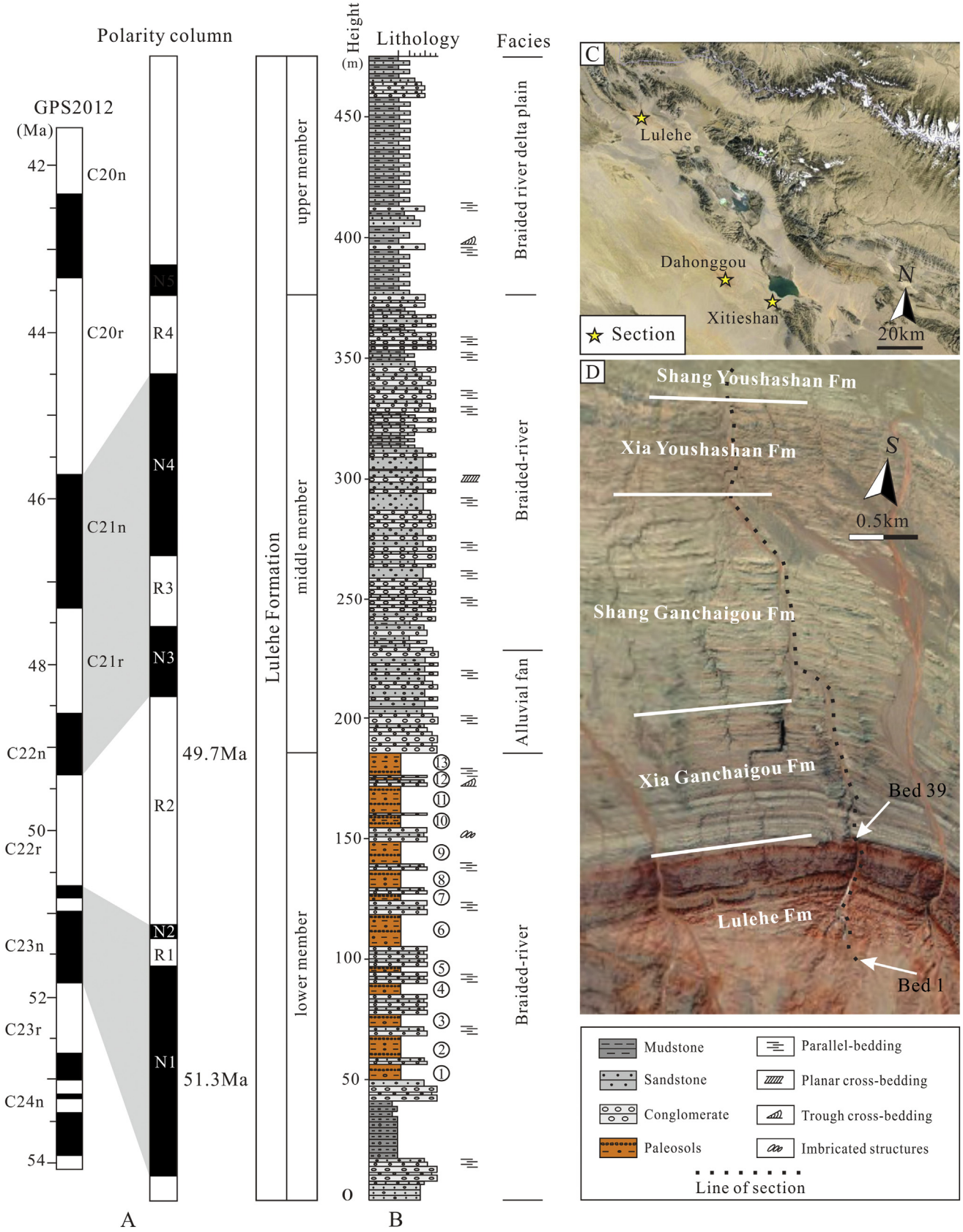

Fig. 2. (A, B) Geochronological (Ji et al., 2017) and stratigraphic framework of the DHG section (circled numbers 1–13 indicate paleosols); (C) Satellite image of study area in the northern Qaidam Basin; (D) Google Earth image (www.earth.google.com) of the studied section.

The present study examines the Dahonggou (DHG) section (37°29′11″N, 95°12′42″E), which is located on the southern limb of the Dahonggou Anticline, on the northern margin of the Qaidam Basin (Fig. 1B). The DHG section has a total thickness of 5400 m belonging to the Lulehe to Shizigou Formations (Song et al., 2013; Ji et al., 2017). This study focuses mainly on the 476-m-thick lower Lulehe Formation (Fig. 2A, B), which is dominated by conglomerates and sandstones interbedded with red mudstones and paleosols.

2.2. Age constraints

A recent paleomagnetic analysis constrained the depositional age of the Lulehe Formation at DHG from ~52.0 to 44.0 Ma (Ji et al., 2017) (Fig. 2A). This age range is consistent with magnetostratigraphic-based estimates for the Lulehe Formation (~53.5 to 43.8 Ma) in the Lulehe section, which is located ~80 km to the northwest of the DHG section (Zhang, 2006; Fig. 2C). In addition, the age of the base of the Lulehe Formation at DHG is consistent with the magnetostratigraphically determined basal age of the Xitieshan section (53.8 Ma), which is ~20 km to the west of DHG (Ke et al., 2013; Fig. 2C).

A recent paleomagnetic study yielded a different interpretation of the age of the Cenozoic fill of the Qaidam Basin. W.T. Wang et al. (2017) analyzed the Honggou section, which is located ~10 km west of DHG, estimating the age of the Lulehe to Shizigou Formations to be ~25.5 Ma to ~4.8 Ma, an age assignment putatively supported by discoveries of mammal fossils in the middle part of the Shang Ganchaigou Formation. Their results imply that the sedimentary fill of the Qaidam Basin is significantly younger than previously thought (QBGMR, 1991; Huang et al., 1996). In our study section (DHG), a distinct shift in ostracod assemblages from freshwater *Ilyocypris* to brackish-water *Cyprideis* in the lower member of the Shang Youshashan Formation (Song et al., 2017) is a marker for the middle Miocene (Sun et al., 1999; Yang et al., 2006; Yang, 2000). On this basis, we correlated the magnetozone record for DHG with the international GPTS (Gradstein et al., 2012) and estimated the base of the DHG section to be at least ~52 Ma in age (Ji et al., 2017). This age assignment is supported by an independent correlation based on the Dynamic Time Warping algorithm (Lallier et al., 2013), and it is consistent with traditional dating of the Qaidam Basin fill (QBGMR, 1991; Huang et al., 1996). Adopting an age range of ~52–44 Ma for the Lulehe Formation, we calculated by linear interpolation that the paleosol interval dates to 51.3–49.7 Ma (Fig. 2A).

2.3. Depositional setting

The Lulehe Formation is well exposed in the northern Qaidam Basin, where it consists mainly of three depositional facies: alluvial fan, braided river, and braided river delta (Fig. 2B; QBGMR, 1991; Bush et al., 2016). The lateral continuity of individual beds is variable, with some extending over tens to hundreds of meters. Previous studies of the Lulehe Formation in the northern Qaidam Basin have inferred a detrital source region to the north, in the South Qilian Mountains (Rieser et al., 2006; Zhuang et al., 2011b; Jian et al., 2013). This inference is consistent with paleocurrent data from the DHG section, in which clast imbrications and cross-bed foresets demonstrate southward to southwestward paleocurrent directions (Song et al., 2013; Ji et al., 2017).

The sedimentary sequence of the Lulehe Formation displays a threefold division into lower, middle, and upper members (Fig. 2B). The lower member consists mainly of conglomerates, sandstones, and mudstones that were deposited in a braided river facies. Conglomerate and sandstone layers commonly exhibit erosional surfaces at their bases and large-scale trough cross-bedding, horizontal bedding, and clast imbrication internally. Thick-bedded conglomerates contain pebble- to cobble-sized clasts and are moderately sorted, which is typical of gravel-bed braided river channels in a braided river setting (Miall, 1996; Fig. 3A). Fine-grained sandstones and pebbly mudstones with dispersed carbonate nodules are typical of overbank (floodplain) deposits that accumulated at relatively slow sedimentation rates (Fig. 3B, C, D) (Miall, 1977, 1996).

The middle member is dominated by alluvial fan and braided river deposits consisting of thick-bedded brownish-red pebble-cobble-sized conglomerates, sandstones, and mudstones. Some of the conglomerates contain pebble- to boulder-sized clasts and are poorly sorted, which is typical of deposition in an upper alluvial fan setting (Miall, 1996) (Fig. 3E). Large-scale planar cross-bedding and horizontal bedding are developed in the conglomerate and sandstone beds. The clast-supported conglomerates and sandstones are interpreted as channel bar deposits of braided streams (Miall, 1977) (Fig. 3F), and mudstones represent overbank (floodplain) deposits (Miall, 1977, 1996).

The upper member mainly consists of tabular conglomerates and brownish-red, medium- bedded, fine-grained sandstones interbedded with thinly-bedded mudstones, which are interpreted as a braided river delta plain facies (Nemec and Steel, 1988). The poorly graded tabular conglomerate beds are interpreted as high-velocity channel deposits that accumulated during the flood stages on the delta plain of a braided river delta system (Benvenuti, 2003). These meter-scale conglomerate beds contain horizontal and trough cross-stratification, which is interpreted to have been produced by lateral accretion of point bars (Miall, 1996; Zhuang et al., 2011b). Interbedded fine-grained sandstones and mudstones are overbank deposits (Fig. 3G).

2.4. Paleosol horizons

A series of 13 paleosol horizons is present in the DHG section between 50 and 180 m (Fig. 2B). Individual paleosols were identified based on vertically elongate rhizoliths, mottles, burrows, carbonate nodules, and weakly developed slickensides (Fig. 3H). The paleosols exhibit visible horizonation, with a weakly developed A horizon above B and C horizons. Most of the A horizons were eroded by overlying fluvial channels. We classified these paleosols as calcisols based on the classification scheme of Mack et al. (1993). We summarize field observations of the paleosols in Table 1.

Individual paleosols range from 1.0 to 13.0 m in thickness and have sharp upper contacts with the overlying braided river channel deposits (Fig. 3B). Gray-white mottles in the form of vertical stripes are developed within the pebbly mudstone layers (Fig. 3C), which are diagnostic features of floodplain deposits deposited at slow sedimentation rates in well-drained, oxygenated environments (Kraus, 1997; Wanas et al., 2015). Abundant pedogenic carbonate nodules in the B horizon suggest that these paleosols were calcisols (Mack et al., 1993) (Fig. 3D). Successive paleosols are commonly separated by two to four pebbly layers. Paleosols preserved in floodplain deposits are commonly complex due to spatial and temporal variations in floodplain sedimentation (Kraus, 1996; McCarthy et al., 1997; Horiuchi et al., 2009). Floodplain paleosols in the Lulehe Formation sometimes contain repeated B horizons, representing complex pedogenic processes and/or a compound soil profile. Such profiles are commonly developed within unstable aggradational systems characterized by intermittent sediment influx interspersed with erosional events (McCarthy et al., 1998).

3. Materials and methods

3.1. Sample collection

A total of 95 pedogenic carbonate nodules for carbon-isotope analysis were collected in situ from 11 paleosol horizons. The samples were collected at depths of 40–50 cm below the overlying channel deposits in order to minimize the effects of atmospheric CO_2 diffusion and evaporation on isotopic compositions (Cerling, 1984; Cerling and Quade, 1993). To minimize the potential influence of recent contamination and weathering, at least 50 cm of material was removed from the exposed surface prior to sample collection. Because marine carbonates have markedly higher $\delta^{13}C$ values compared to continental carbonates

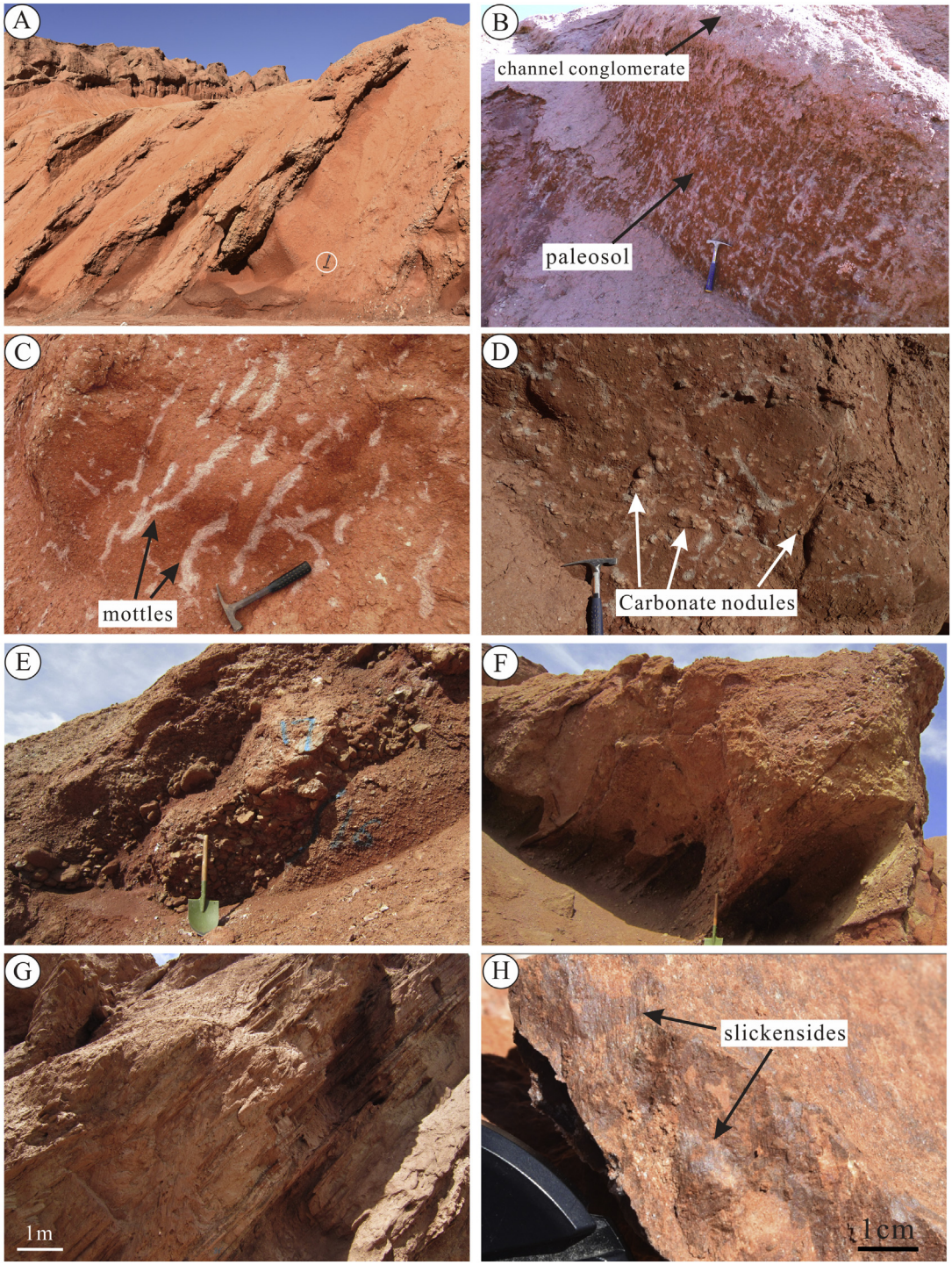

Fig. 3. Outcrops exhibiting various sedimentological facies of the Lulehe Formation. (A) Several gravel-bedded braided river channels. (B) Field view of the paleosols showing sharp contacts with overlying avulsion channel deposits. (C) Reddish-white mottled appearance in the form of downward stripes in sandy mudstones. (D) Dispersed pedogenic carbonate nodules within sandy mudstones. (E) Avulsion channel deposits formed by sheet floods. (F) The well-sorted conglomerates interpreted as channel bar deposits of braided streams. (G) Sandstones intercalated with thinly bedded mudstone. (H) Weakly developed slickensides in sandy mudstones.

(Veizer et al., 1999), their isotope compositions can be used to assess if the adjacent paleosol carbonate nodules are primary or altered (DeCelles et al., 2007; Leier et al., 2009). For this purpose, we analyzed three samples representing reworked limestone clasts from Ordovician and Carboniferous marine units that were collected from fluvial channel deposits of the Lulehe Formation (QBGMR, 1991).

For clay mineralogical analysis, a total of 67 samples averaging ~100 mg each were collected from the matrix of the B and C horizons of the paleosols at an average sampling interval of ~1 m. Variation in sample spacing was due to thickness variations of paleosol horizons.

3.2. Clay mineralogical analysis

Samples for clay mineralogical analysis were dried in an oven overnight at 70 °C. Each sample was ground to powder finer than 74 μm using an agate mortar. Isolation of clay species (< 2 μm fraction)

Table 1
Characteristics of A, B and C horizons of paleosols in the Lulehe Formation at DHG.

Horizons	Color (Munsell hue)	Organic matter (%)	Depth below paleosol surface (cm)	Carbonate nodules (%)	Horizon preservation
A horizon	10R 5/4	< 3	~0–30	–	Poor/partial
B horizon	10R 6/4	< 1	~30–100	20–70	Good
C horizon	2.5YR 5/4 10R 4/6	< 1	–	< 10	Good

followed the procedure of Jackson (1985). Briefly, carbonates were removed using an acid buffer composed of acetic acid and sodium acetate. After washing twice by distilled water, organic matter was removed by using 30% hydrogen peroxide and heating at 90 °C for half an hour. Amorphous iron and aluminum oxides were removed using dithionite-citrate-bicarbonate (DCB). Ca-saturated clay species were recovered by washing the samples three times with 1 mol/l $CaCl_2$, followed by dialysis using a semipermeable membrane. Oriented clay slides of the < 2-μm fractions were produced by pipetting a clay slurry, dispersed by ultrasonic treatment, onto glass slides.

3.2.1. XRD analysis

Preparation of air-dried(AR), ethylene glycol(EG) saturated, and 400 °C- and 600 °C-heated clay samples followed the methods of Hong et al. (2007, 2010a) and Kahle et al. (2002). X-ray diffraction (XRD) patterns were recorded with a Panalytical X'Pert PRO DY2198 diffractometer with Ni-filtered Cu-Ka radiation (40 kV, 40 mA) at the Laboratory of Geological Processes and Mineral Resources, China University of Geosciences-Wuhan. Clay slides were scanned with a step speed of 0.02°2θ/s ranging from 2 to 47° 2θ. Humidity was controlled at 40%RH during the measurements.

Clay minerals were identified by their characteristic reflections in three differently treated XRD patterns (Moore and Reynolds, 1989). Specifically, the characteristic peak of smectite (S) shifted from 15.2 to 16.8 Å after ethylene glycol saturation and then collapsed to 10 Å after heating to 400 °C. The characteristic peaks of chlorite (Ch) are 14.2 Å, 7.1 Å, 4.74 Å, and 3.54 Å. These peaks did not shift after ethylene glycol saturation and heating to 400 °C. The intensity of the peak at 7.1 Å collapsed whereas the 14.2 Å peak was enhanced for chlorite heated to 600 °C. Illite (I) was determined by peaks at 10 Å, 5 Å, and 3.33 Å, and the position of these peaks did not shift after saturation. The 10 Å peak was intensified after heating to 600 °C due to the collapse of smectite layers. Kaolinite was identified by the 7.1 Å and 3.58 Å peaks. The position and strength of these peaks remained stable after saturation or heating to 400 °C, but they disappeared after heating to 600 °C. The presence of irregular mixed-layer illite-smectite minerals was identified based on two broad peaks, with one located between the ~8.4–8.5 Å peak (d_{002} reflection) of smectite and the 10.0 Å peak (d_{001} reflection) of illite, and the second located between the ~5.6 Å peak (d_{003} reflection) of smectite and the 4.9 Å peak (d_{002} reflection) of illite (Fig. 4).

Quantification of clay-mineral proportions was conducted using the program NEWMOD (Reynolds Jr., 1985) with the differences between the fitting results of air-dried and ethylene glycol states within 3%. The clay contents were obtained by curve fitting methods proposed by Reynolds Jr. (1985).

3.2.2. SEM and EDS analysis

Small blocks of bulk samples were selected and platinum-coated for scanning electron microscopic (SEM) observations of mineral morphology. Element relative contents for the selected areas during SEM observations were determined by an energy-dispersive X-ray spectroscopy (EDS) system, with a resolution of 1.0 nm at 15 kV. Both SEM and EDS observations were carried out at the State Key Laboratory of Biogeology and Environmental Geology at the China University of Geosciences-Wuhan using a SU8010 scanning electron microscope.

3.3. Stable-isotope analyses

3.3.1. Paleosol carbonates and limestone clasts

For each paleosol carbonate sample, ~1 mg of powder was collected using a dental drill, with care taken to avoid visible spar phases of pedogenic carbonate nodules. About 150–400 μg of powder was placed in a 10 ml Na-glass vial, sealed with a butyl rubber septum, and reacted with 100% phosphoric acid at 72 °C after flushing with helium. The evolved CO_2 gas was analyzed for $\delta^{13}C$ and $\delta^{18}O$ using a MAT-253 mass spectrometer coupled directly to a Finnigan Gasbench II interface (Thermo Scientific). Isotopic values are reported as per mille variation relative to the Vienna Pee Dee Belemnite (VPDB) standard. Analytical precision was better than ± 0.1‰ for both $\delta^{13}C$ and $\delta^{18}O$ values based on replicate analyses of two laboratory standards: Chinese National Standards GBW04416 ($\delta^{13}C = +1.61‰$, $\delta^{18}O = -11.59‰$) and GBW04417 ($\delta^{13}C = +6.06‰$, $\delta^{18}O = -24.12‰$). Carbon and oxygen analyses were performed at the State Key Laboratory of Biogeology and Environmental Geology of the China University of Geosciences-Wuhan.

3.3.2. Modern meteoric waters

Four river-water samples and one precipitation sample were collected within the Qaidam Basin at Dachaidam Town during the summers (July–August) of 2011 and 2012, respectively (Fig. 1A). The river-water samples were pumped for 5 to 10 min before sampling. Water $\delta^{18}O$ and $\delta^{2}H$ values were determined using a Finnigan MAT-253 mass spectrometer from CO and H_2 gas, respectively, generated by a Thermal Conversion Elemental Analyzer (TC/EA) at 1400 °C (Liu et al., 2010). The $\delta^{18}O$ and $\delta^{2}H$ values were corrected using an internal laboratory standard, "Wuhan water" ($\delta^{18}O = -5.43‰$, $\delta^{2}H = -40‰$), calibrated to Vienna Standard Mean Ocean Water (VSMOW). The precisions of $\delta^{18}O$ and $\delta^{2}H$ measurements are ± 0.1‰ and ± 1.0‰, respectively. These isotopic analyses were performed at the State Key Laboratory of Biogeology and Environmental Geology of the China University of Geosciences-Wuhan.

4. Results

4.1. SEM and EDS results

Illite particles usually occur as discrete clasts with angular and irregular outlines, and aggregates of clay particles usually exhibit a typical swirly texture (Fig. 5A). The EDS spectra for flaky illite are characterized by strong Si and Al and moderate K peaks, consistent with the chemical composition of illite. Observations by SEM reveal that smectite occurs as a major component in most of the paleosol samples. There are two different morphologies of smectites: 1) smectites flakes growing on the surfaces of euhedral platy gypsum crystals (Fig. 5B); and 2) smectites with typical "honeycomb" microstructure (Fig. 5C, D) in sediments with high Si, moderate Al, and lower Ca and Fe peaks. Euhedral platy gypsum is present in most samples and yielded strong Ca and S peaks (Fig. 5B), indicating crystallization directly from solution (i.e., an authigenic origin).

4.2. Clay-mineral assemblages

Typical XRD patterns of the paleosol samples are illustrated in Fig. 5. The XRD analyses show that the clay fraction (< 2 mm) in the Lulehe Formation consists mainly of smectite, illite, chlorite, mixed-layer illite/smectite (I/S), and kaolinite (see Table S1 and Fig. 6). Smectite (20–86%) and mixed-layer I/S (8–53%) are the dominant clay minerals, with average contents of 46% and 36% in the studied paleosol horizons, respectively (Fig. 7). Illite (3–30%) has a slightly lower abundance, with an average of 13%. Kaolinite (0–9%) and chlorite

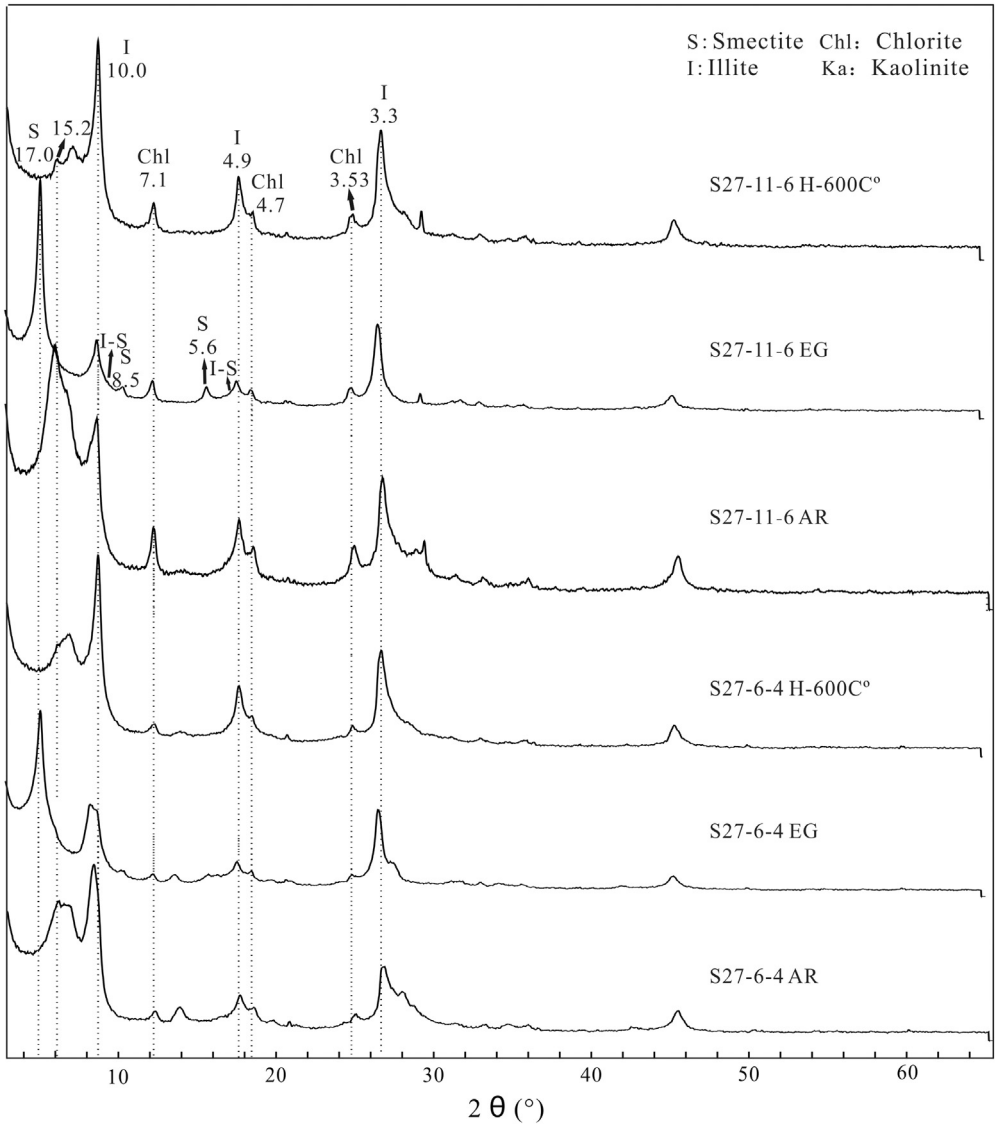

Fig. 4. X-ray diffraction patterns of clay fraction of the representative sample of the Lulehe Formation sediments in the Qaidam Basin.

(0–2%) have even lower abundances, averaging 3% and 1%, respectively.

The amount of smectite is higher in the paleosol horizons than in the siliciclastic sediment layers of the Lulehe Formation. The content of smectite is negatively correlated with that of I/S ($r = -0.84$; p-value < 0.001, $n = 67$) and illite ($r = -0.68$; p-value < 0.001, $n = 67$) in the studied paleosol horizons (Fig. 6). As a comparison, the correlations of smectite with I/S and illite are non-existent to weak in the non-paleosol mudstones of the Lulehe Formation ($r = +0.04$, p-value $= 0.35$, $n = 24$ and $r = -0.46$, p-value < 0.01, $n = 24$, respectively, Fig. 6). The pronounced inverse relationship between illite and smectite (Fig. 6) is likely an indication of illite-to-smectite pedogenic weathering conversions (Hong et al., 2016; Fang et al., 2017).

4.3. Stable-isotope compositions

The $\delta^{18}O_{carb}$ and $\delta^{13}C_{carb}$ values in pedogenic carbonate nodules and reworked marine limestone clasts of the Lulehe Formation are given in Table S2 and shown in Figs. 8 and 9. The $\delta^{18}O_{carb}$ values of pedogenic carbonate nodules range from -7.7 to -10.7‰ with an average of -9.7‰ (VPDB), and the $\delta^{13}C_{carb}$ values range from -5.0 to -9.5‰ with an average of -7.1‰. The $\delta^{18}O$ values of marine limestone clasts range from -7.1 to -9.5‰ with an average of -8.3‰ (VPDB), and the $\delta^{13}C$ values range from -4.1 to -0.9‰ with an average of -2.5‰.

The $\delta^{18}O_w$ and $\delta^{2}H_w$ values of the modern river water and precipitation samples are given in Table S3. The $\delta^{18}O_w$ values of river water range from -7.6 to -10.3‰ with an average of -9.0 ± 1.1‰ (VSMOW). The $\delta^{2}H_w$ values range from -60.5 to -71.5‰ with an average of -64.8 ± 5.2‰. The $\delta^{18}O_w$ and $\delta^{2}H_w$ values of the precipitation are -12.6‰ and –102.7‰, respectively.

5. Discussion

5.1. Diagenetic influences

Several lines of evidence indicate that the isotopic compositions of the lower Eocene paleosol carbonates in the DHG section have not been diagenetically altered. First, we employed the “isotope conglomerate test” (DeCelles et al., 2007). Three reworked marine limestone clasts from stratigraphically adjacent beds yielded $\delta^{18}O$ and $\delta^{13}C$ values that fall within the range expected for unaltered Carboniferous and Ordovician marine carbonates (Veizer et al., 1999), indicating that the isotopic compositions of these reworked clasts have not been altered

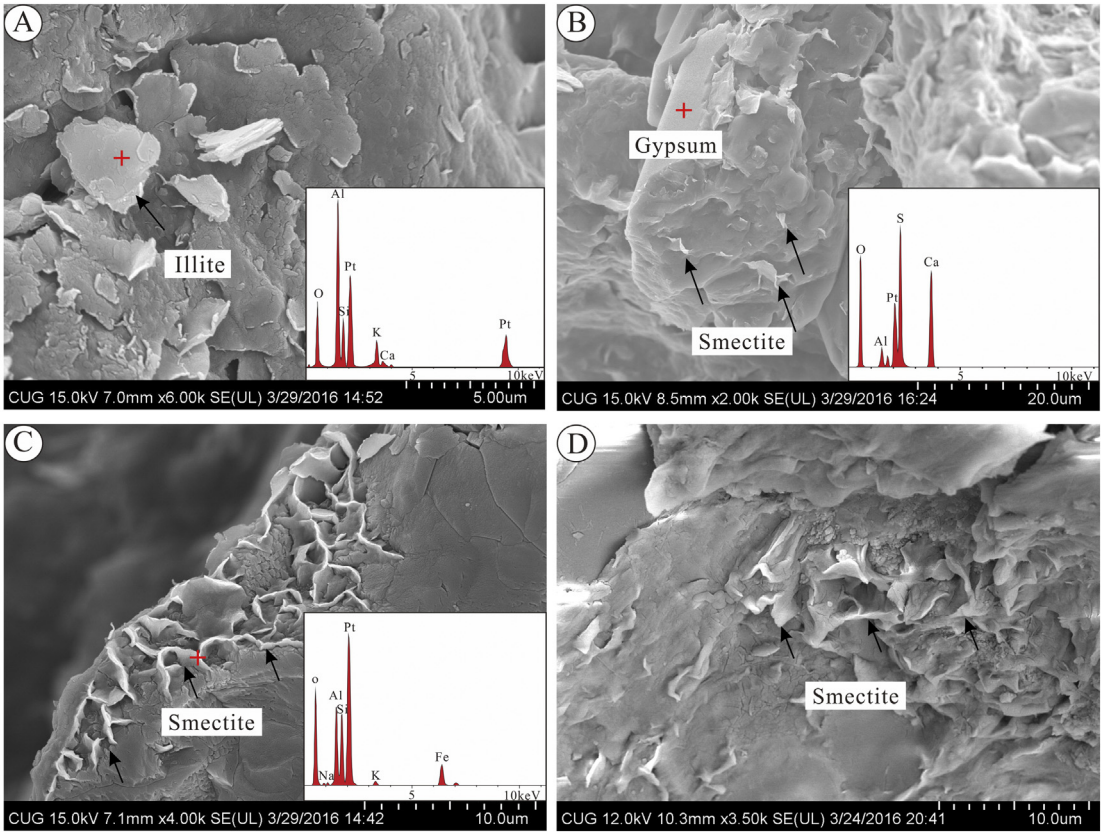

Fig. 5. SEM and EDS images of clay minerals in paleosol horizons of Lulehe Formation showing: (A) Detrital illite particles with swirl texture; (B) smectites flakes grown on the surface of euhedral platy gypsum crystal; (C, D) authigenic smectite minerals with typical"honeycomb"structure within a micro-crack.

(Fig. 9). This result suggests that the pedogenic carbonates also may not have experienced digenetic alteration of their primary $\delta^{18}O_{carb}$ and $\delta^{13}C_{carb}$ values. Second, late-stage diagenesis would have shifted the $\delta^{18}O_{carb}$ to more negative values with increasing burial depth (due to elevated temperatures) (Wang et al., 2012), which is not seen in our data (Fig. 8). Third, based on analysis of sandstone compaction, Zhuang et al. (2011a) inferred that diagenetic effects were minor up to ~5000 m depth in the northern Qaidam Basin. Fourth, based on the isotopic signatures of middle Eocene marine mollusk shells, Kent-Corson et al. (2009) inferred only minor diagenetic alteration of carbonates in northern Tibetan Plateau basins, including the Qaidam Basin (cf. Li et al., 2016). Fifth, isotopic compositions within our sample suite do not display any systematic stratigraphic trends (e.g., decreasing $\delta^{18}O$ values with depth) that could be attributed to burial diagenesis (Currie et al., 2016). Finally, in the DHG section, smectite is present in all six formations including the studied paleosol interval (Hong et al., 2010b), suggesting a minimal influence of burial diagenesis. Based on these considerations, we infer that the isotopic values of pedogenic carbonate nodules in the DHG section can be regarded as primary and therefore can be used to reconstruct paleoclimate and paleoelevation changes.

5.2. Origin of clay minerals

Smectite minerals commonly form under climatic conditions characterized by a strong alternation between warm-wet and cool-dry seasons (Singer, 1984). Although early diagenesis of volcanic glass or volcanic rocks is an important process for creating authigenic smectites (Chamley, 1989), no volcanic or volcaniclastic components are present in the DHG section. SEM observations reveal features that are consistent with authigenic smectite formation in soils, including typical "honeycomb" structure within micro-cracks (Fig. 5C, D) (Wilson and Pittman, 1977; Chamley, 1989). In addition, smectite flakes can be seen growing on the surfaces of gypsum crystals (Fig. 5B), indicating that smectite formation post-dated gypsum precipitation, and that smectite therefore precipitated from fluids during the soil-forming process. Moreover, smectite contents are negatively correlated with illite and I/S contents (Fig. 6), suggesting that smectite formed during chemical weathering through transformation of illitic precursor minerals (Setti et al., 2014). Finally, as smectite is commonly altered to illite in sedimentary basins that have reached intermediate thermal ranks (89–116 °C), its abundant presence places a limit on the maximum burial temperatures of the study section (Pollastro, 1993; Kubler, 1997). Thus, microscopic observations and bulk clay-mineral compositions provide strong evidence that smectite in the paleosol horizons of the Lulehe Formation was largely an authigenic product of pedogenesis.

Illite, in contrast, had a predominantly detrital origin, as shown by the swirly texture of the clay aggregates and the discrete clay particles with angular and irregular outlines (Fig. 5A). Additionally, illite abundance is considerably lower in the paleosols (average 13.3%) than in the non-paleosol samples (average 49%) (Fig. 6). Thus, illite in the studied section is mainly of detrital origin.

Kaolinite forms as a result of strong chemical weathering on land and is considered to be the end-product in intensely weathered in situ soil profiles (Chamley, 1989). In the studied paleosol horizons, kaolinite is a minor component of clay-mineral assemblages, averaging 2.9% (Fig. 7). The small amounts of kaolinite imply that weathering intensity in the hinterlands was not high enough to form large amounts of this mineral.

5.3. Paleoclimate implications of bulk clay-mineral assemblages

Clay minerals have been frequently used as indicators of pedogenesis because the mineralogy of the clay fraction in soils is closely related to weathering processes (C.W. Wang et al., 2017). The nature and

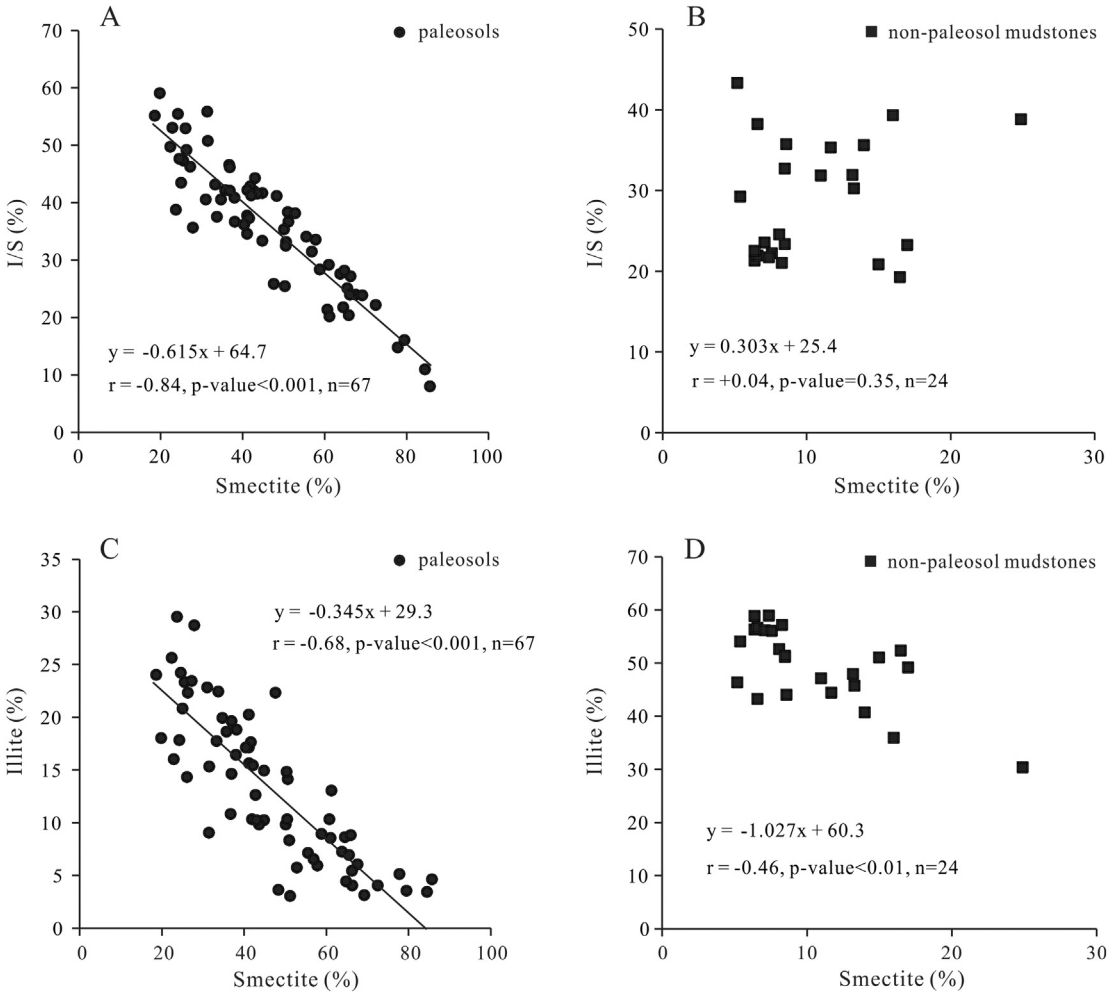

Fig. 6. Clay-mineral relationships in the DHG section. Smectite versus I/S in paleosol horizons (A) and non-paleosol mudstone (B); smectite versus illite in the paleosol horizons (C) and non-paleosol mudstone (D).

intensity of chemical weathering processes in soils are strongly influenced by climate, especially temperature and precipitation. The marked difference in clay-mineral composition between the matrix of the paleosols and non-paleosol mudstone samples suggests that pedogenetic processes were an important influence on the composition of the clay-mineral assemblages in paleosols of the Lulehe Formation.

Smectites in the studied paleosol horizons are mainly of pedogenic origin, generated through intense chemical weathering (see Section 5.2). Pedogenic smectite is commonly found in monsoonal regions characterized by strongly seasonal precipitation (Sheldon and Tabor, 2009). Thus, the abundant smectite in the study units is an indication of pronounced seasonality of climate conditions on the northern Tibetan Plateau margin during the Eocene.

Kaolinite is a chemical weathering product of warm-humid climate conditions, whereas illite and chlorite are mostly generated through physical weathering of bedrock under cool/temperate to cool/dry conditions (Chamley, 1989; Nesbitt and Young, 1984). In the studied paleosol horizons, kaolinite/illite ratios are generally high, indicating relatively intense chemical weathering and thus consistent with the abundant occurrence of pedogenic smectite.

In summary, bulk clay mineralogy indicates that the formation of Lulehe Formation paleosols was a result of pronounced seasonality, with chemical weathering primarily during warm-wet seasons. A consistent relationship between pedogenic smectite abundance and high benthic foraminiferal $\delta^{18}O$ values (Fig. 10A) indicates that a pronounced wet-warm climate regime existed throughout the interval of accumulation of the study section, which is also supported by high kaolinite/illite ratios (Fig. 10B). This inferred wet-warm climate regime is consistent with globally elevated temperatures of the Early Eocene Climatic Optimum (EECO) (Fig. 10), which was a period of extreme global warmth (Zachos et al., 2001, 2008) characterized by higher globally averaged temperature and precipitation levels than today (Shackleton and Boersma, 1981; Miller et al., 1987; Zachos et al., 2001; Pearson et al., 2007; Bijl et al., 2009; Hollis et al., 2009, 2012).

5.4. Significance of soil carbonate nodules

Carbon isotopic compositions can provide insights into the origin of soil carbonate nodules and contemporaneous atmospheric CO_2 levels. In the Lulehe Formation, soil nodules yield $\delta^{13}C$ values that are distinctly more negative (by ~1 to 6‰) than those of co-occurring fluvial cements in the Lulehe Formation (average $\delta^{13}C = -4.46$‰) (Sun, 2014) (Figs. 8-9). We suggest that this negative offset was due mostly to a smaller influence of evaporated soil waters on the paleosol carbonates than on the fluvial cements and, possibly, to less recycling of carbon from detrital marine limestone clasts. The difference in $\delta^{13}C$ values is consistent with authigenic formation of the carbonate nodules during pedogenesis.

Soil carbonate $\delta^{13}C$ is a function of the $\delta^{13}C$ of soil CO_2 at the time of precipitation (Cerling, 1984). Key influences on the $\delta^{13}C$ values of soil CO_2 are the relative fractions of C3- versus C4-derived organic matter, soil respiration rate, and paleo-atmospheric pCO_2 (Cerling,

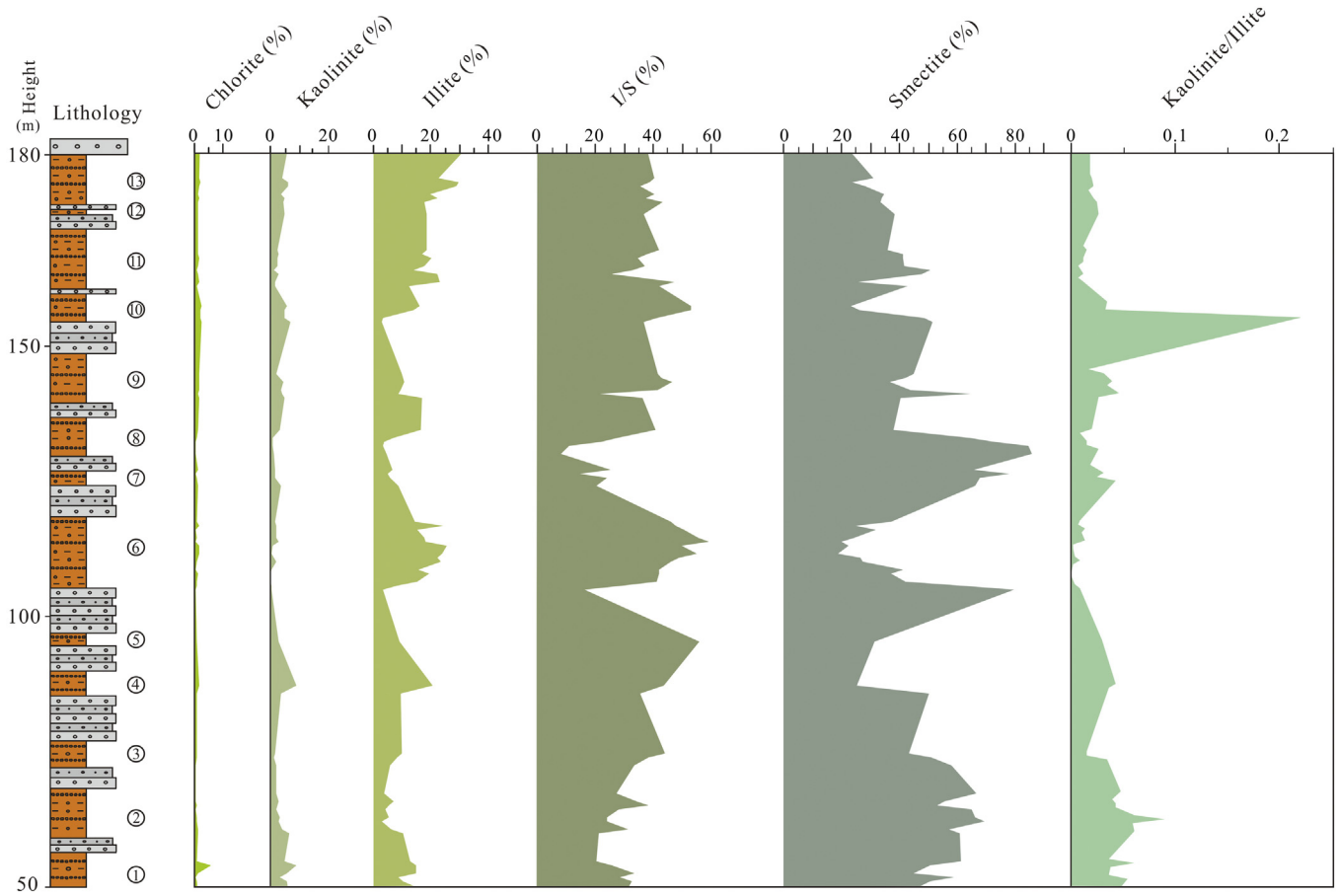

Fig. 7. Profiles of clay-mineral content and kaolinite/illite ratios in paleosol horizons of Lulehe Formation. Circled numbers 1–13 indicate paleosols.

1991; Cerling and Quade, 1993; Koch, 1998). Carbonate nodules in modern soils precipitated in equilibrium with CO_2 derived solely from C_3 plants have $\delta^{13}C$ values ranging from −9 to −13‰, whereas carbonate nodules precipitated in equilibrium with CO_2 derived solely from C_4 plants have $\delta^{13}C$ values ranging from +1 to +3‰ (Cerling and Quade, 1993). Soil temperature has a minimal effect on these fractionations (Koch, 1998). There is no evidence for the widespread presence of C_4 plants in the early Eocene (Cerling and Quade, 1993; Strömberg, 2011), making C_4 plant inputs an unlikely cause of ^{13}C-enriched soil carbonate in the Lulehe Formation.

Changes in soil respiration rate are also an unlikely control: the higher $\delta^{13}C$ values of Lulehe Formation soil nodules (mean −7.1 ± 0.8‰) compared to modern C_3-plant-derived soil nodules (−9 to −13‰) would require relatively low soil respiration rates. However, previous pollen studies of the Lulehe Formation have found that broad-leaved trees and thermophilic vegetation were dominant in the early Eocene Qaidam Basin (Lu et al., 2010; Song et al., 2013). This paleoflora is consistent with subtropical climatic conditions and suggests an open woodland biome, which would have had higher significantly higher soil respiration rates than the shrub-herb biome in the modern Qaidam Basin. Another possible influence, changes in the $\delta^{13}C$ composition of atmospheric CO_2 is also unlikely because the $\delta^{13}C$ of CO_2 in the early Eocene atmosphere was < 1‰ different from the modern value (Tipple et al., 2010). Therefore, we infer that the relatively ^{13}C-enriched composition of Lulehe Formation soil nodules was the product of higher atmospheric pCO_2 during the early Eocene.

Atmospheric pCO_2 is thought to have been higher during the Early Eocene Climatic Optimum (EECO) at 52–50 Ma (Zachos et al., 2008). Elevated atmospheric pCO_2 has been inferred from studies of marine boron (Demicco et al., 2003), CSM and RegCM3 modeling (Shellito et al., 2003; Thrasher and Sloan, 2009), evaporite minerals (Lowenstein and Demicco, 2006), pedogenic carbonates (Yapp, 2004; Hyland et al., 2013), and stomatal indices (Retallack, 2001a, 2001b; Smith et al., 2010), although the estimated absolute concentrations of pCO_2 vary.

5.5. Paleoelevation implications

The oxygen isotopic composition of soil carbonate is strongly influenced by the isotopic composition of local precipitation in well-drained soils, provided that precipitation is the dominant source of soil water (Cerling, 1984). Therefore, the oxygen isotope composition of pedogenic carbonates growing in hydrologically open systems can be used to reconstruct that of the source meteoric water and, thus, paleoelevations, which are related to meteoric $\delta^{18}O$ via the "altitude effect" (Quade et al., 2007). It is important to understand moisture sources to the northern Tibetan Plateau in order to derive reliable paleoelevation estimates for the Eocene Qaidam Basin. In the modern, the Tibetan Plateau exhibits three distinct climatic domains: (1) the northern domain, which is under the dominant influence of the Westerlies, (2) the southern domain, which is under the dominant influence of the Indian Monsoon, and (3) the transitional domain between them, in which both the Westerlies and Indian Monsoon are influential (Yao et al., 2013). Based on its $\delta^{18}O$ composition, modern precipitation on the northern Tibetan Plateau is sourced mainly from the Westerlies (Yao et al., 2013), and spatial variation in paleo-precipitation $\delta^{18}O$ indicates that the Westerlies have been the dominant moisture source in Central Asia since at least the early Eocene (Caves et al., 2015). For these reasons, we assume that the main moisture source to the Eocene Qaidam Basin was the Westerlies.

In order to calculate the oxygen-isotopic compositions of soil waters ($\delta^{18}O_{psw}$) in isotopic equilibrium with soil carbonate nodules, it is necessary to first estimate the temperature of soil carbonate precipitation

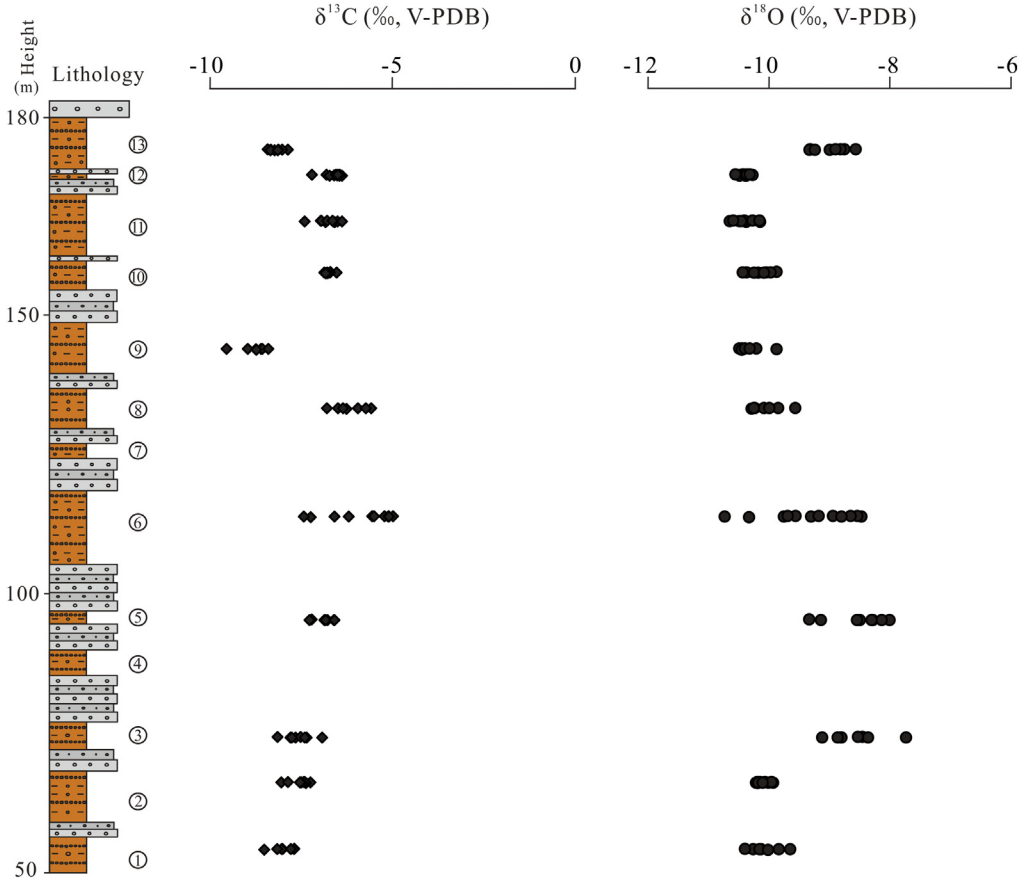

Fig. 8. Profiles of $\delta^{18}O$ and $\delta^{13}C$ in paleosol horizons of Lulehe Formation. Circled numbers 1–13 indicate paleosols.

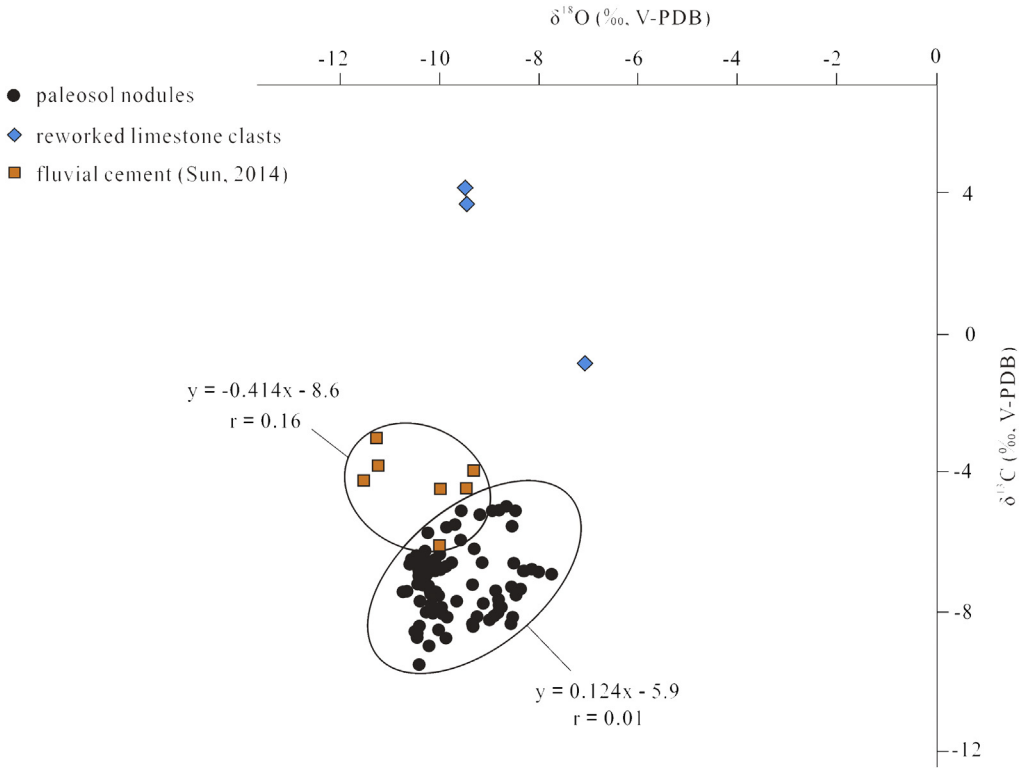

Fig. 9. Carbonate $\delta^{18}O$ versus $\delta^{13}C$ for the DHG section. Shown for comparison are reworked marine limestone clasts from avulsion channel deposits and fluvial cements (Sun, 2014).

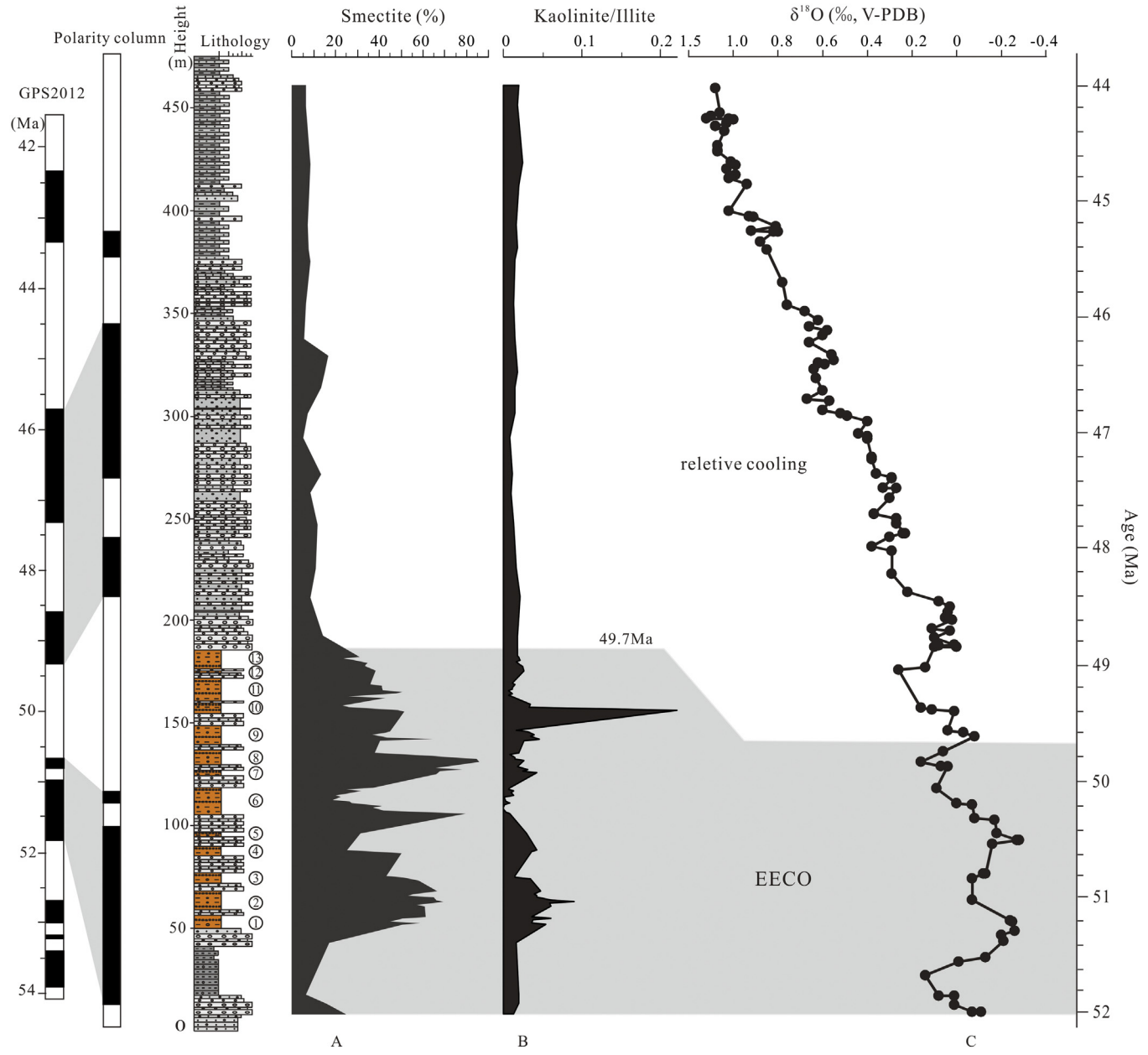

Fig. 10. Relative contents of smectite (a) and kaolinite/illite ratio (b) of the DHG section compared with a multisite composite benthic foraminiferal $\delta^{18}O$ record (c) (Zachos et al., 2001).

(Hoke et al., 2014). Clumped isotope studies have shown that soil carbonate formation is strongly biased towards the warm season (Breecker et al., 2009; Passey et al., 2010; Eren, 2011; Meyer et al., 2014; but see Peters et al., 2013, and Gallagher and Sheldon, 2016, for exceptions). Carbonate nodules on the modern Tibetan Plateau are known to form in the warmest months of the year (Quade et al., 2011, 2013; Huntington et al., 2015), and we therefore assume that soil carbonate formation in the Eocene Qaidam Basin was also biased towards the warm season. During the early Eocene, continental interiors were characterized by generally warm conditions, with summer highs up to 28 °C in the Paris Basin, France (Andreasson and Schmitz, 1996), ~30 °C in the Wind River Basin (Fan et al., 2011), and 30–35 °C in the Bighorn Basin (Snell et al., 2013; the latter two basins both being located in Wyoming, western United States). A similar temperature (~28 °C) was inferred for precipitation of carbonate nodules in Eocene paleosols of the high Tibetan Plateau by Quade et al. (2011). Given these considerations, we assumed a summer temperature of 30 ± 5 °C for the early Eocene Qaidam Basin, which is ~5 °C warmer than calcite precipitation temperatures in modern Tibetan Plateau lakes (~25 ± 5 °C; Lister et al., 1991; Fontes et al., 1996; Zhuang et al., 2011a).

$\delta^{18}O_{psw}$ in the early Eocene Qaidam Basin can be calculated from the $\delta^{18}O$ of soil carbonate nodules in the Lulehe Formation. The fractionation factor (α) between paleo-meteoric waters and soil carbonate is defined as: $\alpha_{(calcite\text{-}water)} = (1000 + \delta^{18}O_{calcite}) / (1000 + \delta^{18}O_{water})$. The equation to calculate α is: $1000\ln(\alpha)_{(calcite\text{-}water)} = 18.03 \times 10^3 T^{-1} - 32.42$, where T is in degrees Kelvin (Kim and O'Neil, 1997). The equation to calculate $\delta^{18}O_{(SMOW)}$ from $\delta^{18}O_{(VPDB)}$ is: $\delta^{18}O_{(SMOW)} = 1.03091 \times \delta^{18}O_{(VPDB)} + 30.91$ (Coplen et al., 1983). We used the mean $\delta^{18}O_{carb}$ value of paleosol carbonates (−9.7 ± 0.9‰) and mean summer temperature of 30 ± 5 °C to calculate the $\delta^{18}O$ of paleo-meteoric water, yielding values of −7.3 to −5.4‰ (VSMOW). This range of estimates takes into account uncertainties related to both variations in O-isotopic measurements and

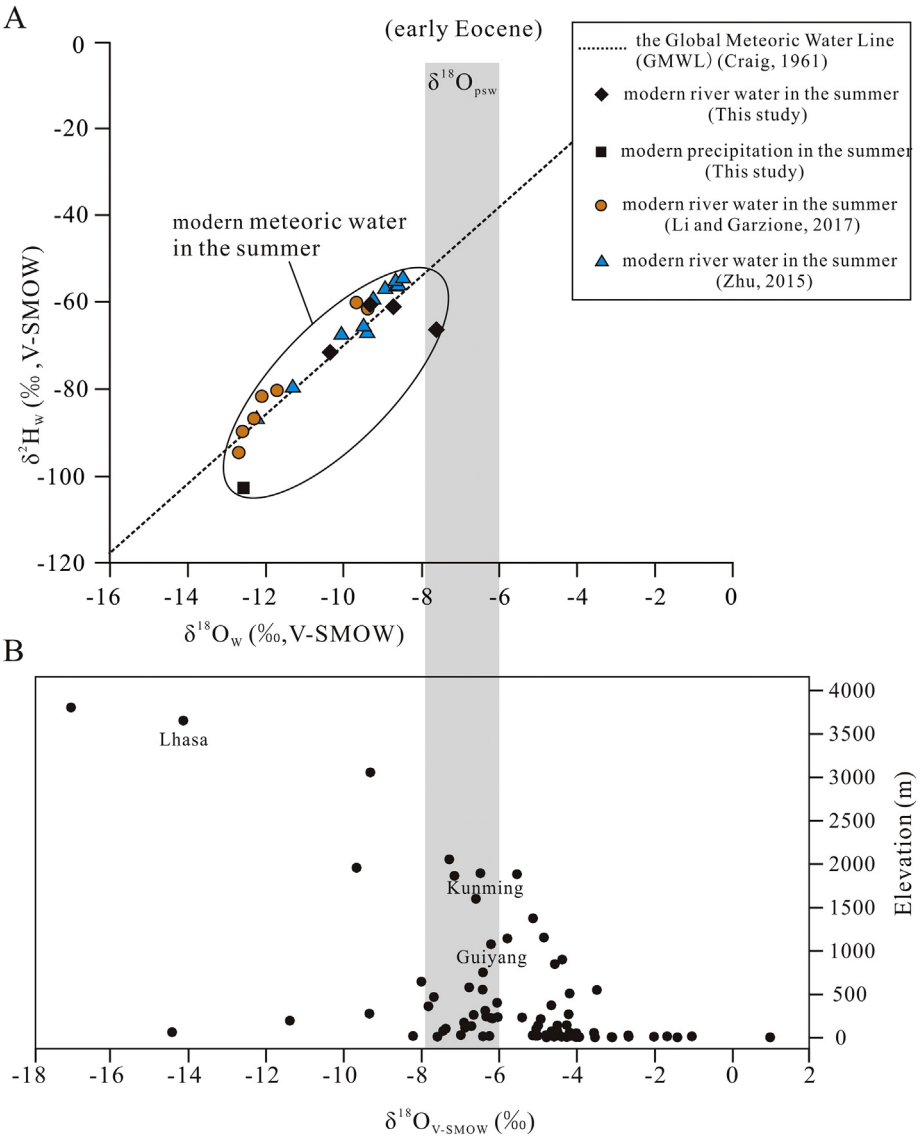

Fig. 11. (A) $\delta^{18}O_w$ vs δ^2H_w plot of modern groundwater and precipitation samples (this study, Li and Garzione, 2017, and Zhu, 2015) collected from the Qaidam Basin during the summer, as compared with the calculated $\delta^{18}O_{psw}$ (paleo-surface water) values during the early Eocene. The GMWL (Craig, 1961) is also shown for reference. (B) Weighted mean annual values of $\delta^{18}O$ (VSMOW) from the Global Network of Isotopes in Precipitation (GNIP) (values from IAEA and WMO, 2012).

inaccuracies in estimated temperatures of soil nodule precipitation.

Additional corrections to $\delta^{18}O_{psw}$ are needed to account for changes in global seawater $\delta^{18}O$ and changes in latitude of the Qaidam Basin since the Eocene. Because of the buildup of continental ice sheets, the oxygen isotope value of seawater has changed by approximately +1‰ since the Eocene (Zachos et al., 1994). The Qaidam Basin was located at 24.7 ± 8°N (Wu et al., 2002) or 27.4°N (Wang, 2006) in the early Cenozoic, which is ~10–12° south of its present latitude of 37°N. The northward shift of the Qaidam Basin requires an adjustment of about −1.6‰ to $\delta^{18}O_{psw}$ to account for the empirical "latitude effect" of Bowen and Wilkinson (2002). Incorporating these two corrections, the $\delta^{18}O$ values of paleo-meteoric water in the Eocene Qaidam Basin were about −7.9‰ to −6.0‰ (VSMOW).

Summer rainfall in the modern Qaidam Basin has a $\delta^{18}O$ value of −10.2 ± 1.6‰ (Fig. 11A). The calculated $\delta^{18}O_{psw}$ value for the early Eocene is ~3.3 ± 1.0‰ higher than that of modern meteoric waters (Fig. 11A). This isotopic difference may be due to (1) a change in meteoric precipitation $\delta^{18}O$ in the Qaidam Basin since the early Eocene, or (2) ^{18}O enrichment of pedogenic carbonates through kinetic fractionation effects related to evaporation (Cerling, 1984; Quade et al., 1989). We infer that kinetic fractionation effects are unlikely because the soil samples were collected from a depth of 40–50 cm below the overlying channel deposits, which should have minimized the effects of evaporation on soil water $\delta^{18}O$ compositions. In addition, the lack of correlation between $\delta^{18}O$ and $\delta^{13}C_{carb}$ in the soil carbonate nodules ($r = +0.01$; p-value > 0.05) (Fig. 5) suggests that evaporation was not an important process on the floodplain, assuming that local rainfall was the dominant source of water for pedogenic carbonates. In addition, experimental and theoretical studies have shown that evaporation has a minimal effect on the $\delta^{18}O$ values of soil water below 30–50 cm in most soils (Xiao et al., 2011; Hough et al., 2014). Thus, we interpret this pronounced difference in $\delta^{18}O$ (~3.3 ± 1.0‰) to have been the result of changes in meteoric $\delta^{18}O$ values between the early Eocene and the modern (Fig. 11A).

An alternative explanation for the 3.3 ± 1.0‰ negative shift in $\delta^{18}O$ is a temperature change. Temperature change affects the $\delta^{18}O$ of freshwater carbonates in two ways: (1) by altering the oxygen isotope fractionation between carbonate and water, and (2) by affecting the $\delta^{18}O$ of source water (i.e., meteoric water). First, the oxygen isotope fractionation between calcite and water varies by ~0.23‰/°C (Kim and

O'Neil, 1997). Second, based on the IAEA/WMO global network, there is a strong positive correlation (~0.58‰/°C) between the long-term annual means of ^{18}O content in precipitation and surface air temperature (Rozanski et al., 1993). Therefore, the combined effect of temperature changes on carbonate $\delta^{18}O$ values is ~0.35‰/°C. In this study, the ~3.3 ± 1.0‰ negative shift in mean $\delta^{18}O$ values in the Qaidam Basin from the early Eocene to the modern is equivalent to an overall cooling of ~10.0 °C. However, reconstructions of sea-surface temperatures (SSTs) based on planktonic foraminifer $\delta^{18}O$ values indicate that low-latitude SSTs have remained nearly constant throughout the Cenozoic (Zachos et al., 1994), and the location of the early Eocene Qaidam Basin in the subtropics (~25–27°N) means that its summer temperatures would not have been much different than at present, and certainly not 10.0 °C warmer. Thus, a change in temperature alone cannot explain the observed large negative $\delta^{18}O$ shift.

The "altitude effect" leads to decreasing $\delta^{18}O$ values with increasing elevation through Rayleigh distillation of meteoric waters (Rozanski et al., 1993). A viable explanation for the ~3.3 ± 1.0‰ negative oxygen isotopic shift since the Eocene is a change in meteoric water $\delta^{18}O$ within the Qaidam Basin catchment as a result of overall uplift. This inference is supported by $\delta^{18}O$ records from the western Qaidam and Gyirong basins, which show large negative $\delta^{18}O$ shifts associated with uplift of the Altun Shan and East Kunlun Range at ~15–14 Ma (Li et al., 2016). In the Gyirong Basin, an abrupt increase in the $\delta^{18}O$ values of lacustrine/fluvial carbonates at 5.5 Ma also reflects a major change in drainage and depositional setting (Wang et al., 2012). Thus, we interpret the marked $\delta^{18}O$ shift in the present study units as due to a lowering of meteoric water $\delta^{18}O$ in consequence of significant uplift of the northern Qaidam Basin since the early Eocene.

The inferred ~5 °C cooling of summer temperatures since the early Eocene can be used to constrain elevation changes of the northern Qaidam Basin. Given an early Eocene mean atmospheric lapse rate of −5.6 °C/km (Song et al., 2010), the ~5 °C cooling is equivalent to an uplift of nearly 1000 m. Relative to its present average elevation of ~3000 m, our calculation implies that the paleo-Qaidam Basin was at an elevation of ~2000 m in the early Eocene. In addition, comparisons between the $\delta^{18}O$ values of modern and paleo-surface waters can be used to evaluate secular changes in surface elevations (Rowley and Garzione, 2007). For this purpose, we made use of modern meteoric water isotope data (i.e., annual averages weighted by precipitation amount) of Global Network of Isotopes in Precipitation (GNIP) sites in Asia (IAEA and WMO, 2012). The calculated $\delta^{18}O_{psw}$ value of −7.9‰ to −6.0‰ for the Eocene Qaidam Basin is in the same range as modern surface waters at elevations of 50–2000 m asl (Fig. 11B). The high $\delta^{18}O_{psw}$ values calculated from early Eocene Qaidam Basin soil nodules are therefore also consistent with a substantially lower paleoelevation. Our paleoelevation estimate is similar to one (~1500 m) based on the $\delta^{18}O$ of Eocene Qaidam Basin lacustrine carbonates (Li et al., 2017). Moreover, palynological assemblages and magmatic geochemistry provide independent evidence of relatively low paleoelevations in the late Eocene (50–35 Ma) Qaidam Basin (Miao et al., 2016; Chen et al., 2018). Stable hydrogen isotopic data indicate that the Qaidam Basin did not attain its present high elevation until the early Late Miocene (Zhuang et al., 2014). Paleomagnetic evidence documents widespread uplift across the northern Tibet region after ~15 Ma (Lu et al., 2016). Hence, all of these observations are consistent with a relatively low paleoelevation (~2000 m) in the early Eocene Qaidam Basin.

6. Conclusions

The present clay mineralogical and stable isotope study of early Eocene paleosols from the Lulehe Formation of the Qaidam Basin yields the following conclusions:

1. The clay-mineral assemblages of the paleosols consist predominantly of smectite and mixed-layer I/S minerals. These clay-mineral suites reveal that the early Eocene Qaidam Basin had a strongly seasonal climate, with a warm-wet summer. Large amounts of pedogenic smectite in the paleosols reflect intensified weathering during the Early Eocene Climatic Optimum (EECO).

2. The $\delta^{13}C$ values of Lulehe Formation pedogenic carbonates (mean −7.1 ± 0.8‰) reflect higher atmospheric pCO_2 during the early Eocene, which is consistent with previous atmospheric pCO_2 estimates for the EECO.

3. The calculated value of soil water $\delta^{18}O$ ($\delta^{18}O_{psw}$) for the early Eocene is significantly higher (by 3.3 ± 1.0‰) than modern summer meteoric waters in the Qaidam Basin. We interpret this marked shift as indicating a decrease in the $\delta^{18}O$ of meteoric water in the catchment area due to a substantial uplift of the northern Qaidam Basin since the early Eocene. The estimated temperature difference (~5.0 °C cooling) implies uplift of the study area by nearly 1000 m, based on an early Eocene atmospheric lapse rate of −5.6 °C/km, to its current average elevation of ~3000 m above sea level.

Supplementary data to this article can be found online at https://doi.org/10.1016/j.palaeo.2018.03.027.

Acknowledgments

We are grateful to Jiaxuan Wang, Gaolei Jiang, Xue Ke, Zenglian Xu and Ruiming chen for field assistance and Yibo Yang, Ke Yin and Chengcheng Ye for their valuable suggestions. This work is funded by the National Natural Science Foundation of China (Grant Nos. 41702118, 41602037, 41702363 and 41772107) and the Geological Survey of China (No. 121201004000150013). We thank the editors and three anonymous reviewers for their constructive suggestions that improved this manuscript.

References

Abels, H.A., Dupont-Nivet, G., Xiao, G.Q., Bosboom, R., Krijgsman, W., 2011. Step-wise change of Asian interior climate preceding the Eocene–Oligocene Transition (EOT). Paleogeogr. Paleoclimatol. Paleoecol. 299, 399–412.
Andreasson, F.P., Schmitz, B., 1996. Winter and summer temperatures of the early middle Eocene of France from *Turritella* $\delta^{18}O$ profiles. Geology 24, 1067–1070.
Benvenuti, M., 2003. Facies analysis and tectonic significance of lacustrine fan-deltaic successions in the Pliocene–Pleistocene Mugello Basin, Central Italy. Sediment. Geol. 157, 197–234.
Bijl, P.K., Schouten, S., Sluijs, A., Reichart, G., Zachos, J.C., Brinkhuis, H., 2009. Early Palaeogene temperature evolution of the southwest Pacific Ocean. Nature 461, 776–779.
Bowen, G.J., Wilkinson, B., 2002. Spatial distribution of $\delta^{18}O$ in meteoric precipitation. Geology 30, 315–318.
Breecker, D., Sharp, Z.D., McFadden, L., 2009. Seasonal bias in the formation and stable isotope composition of pedogenic carbonate in modern soils from central New Mexico, USA. Geol. Soc. Am. Bull. 121, 630–640.
Bush, M.A., Saylor, J.E., Horton, B.K., Nie, J.S., 2016. Growth of the Qaidam Basin during Cenozoic exhumation in the northern Tibetan Plateau: inferences from depositional patterns and multiproxy detrital provenance signatures. Lithosphere 8, 58–82.
Caves, J.K., Winnick, M.J., Graham, S.A., Sjostrom, D.J., Mulch, A., Chamberlain, C.P., 2015. Role of the westerlies in Central Asia climate over the Cenozoic. Earth Planet. Sci. Lett. 428, 33–43.
Cerling, T.E., 1984. The stable isotopic composition of modern soil carbonate and its relationship to climate. Earth Planet. Sci. Lett. 71, 229–240.
Cerling, T.E., 1991. Carbon dioxide in the atmosphere. Am. J. Sci. 291, 377–400.
Cerling, T.E., Quade, J., 1993. Stable carbon and oxygen isotopes in soil carbonates. Geophys. Monogr. 78, 217–231.
Chamley, H., 1989. Clay Sedimentology. Springer, New York (623 pp).
Chang, H., Li, L.Y., Qiang, X.K., Garzione, C.N., Pullen, A., An, Z.S., 2015. Magnetostratigraphy of Cenozoic deposits in the western Qaidam Basin and its implication for the surface uplift of the northeastern margin of the Tibetan Plateau. Earth Planet. Sci. Lett. 430, 271–283.
Chen, J.L., Yin, A., Xu, J.F., Dong, Y.G., Kang, Z.Q., 2018. Late Cenozoic magmatic inflation, crustal thickening, and > 2 km of surface uplift in central Tibet. Geology 46, 19–22.
Cheng, Y.M., Yang, X.N., 2016. Miocene woods from the Qaidam Basin on northern Qinghai-Tibet Plateau with implications for paleoenvironmental change. J. Asian Earth Sci. 116, 198–207.
Coplen, T.B., Kendall, C., Hopple, J., 1983. Comparison of stable isotope reference samples. Nature 302, 236–238.
Craig, H., 1961. Isotopic variations in meteoric waters. Science 133, 1702–1708.
Currie, B.S., Polissar, P.J., Rowley, D.B., Ingalls, M., Li, S.Y., Olack, G., Freeman, K.H., 2016. Paleoaltimetry of the Early Miocene-Pliocene Oiyug basin, southern Tibet. Am. J. Sci. 316, 401–436.

DeCelles, P.G., Quade, J., Kapp, P., Fan, M.J., Dettman, D.L., Ding, L., 2007. High and dry in central Tibet during the Late Oligocene. Earth Planet. Sci. Lett. 253, 389–401.
Demicco, R.V., Lowenstein, T.K., Hardie, L.A., 2003. Atmospheric pCO_2 since 60 Ma from records of seawater pH,calcium, and primary carbonate mineralogy. Geology 31, 793–796.
Dettman, D.L., Fang, X.M., Garzione, C.N., Li, J.J., 2003. Uplift-driven climate change at 12 Ma: a long δ18O record from the NE margin of the Tibetan plateau. Earth Planet. Sci. Lett. 214, 267–277.
Ding, L., Xu, Q., Yue, Y., Wang, H.Q., Cai, F.L., Li, S., 2014. The Andean-type Gangdese Mountains: paleoelevation record from the Paleocene-Eocene Linzhou Basin. Earth Planet. Sci. Lett. 392, 250–264.
Dupont-Nivet, G., Krijgsman, W., Langereis, C.G., Abels, H.A., Dai, S., Fang, X.M., 2007. Tibetan plateau aridification linked to global cooling at the Eocene–Oligocene transition. Nature 445, 635–638.
Dupont-Nivet, G., Hoorn, C., Konert, M., 2008. Tibetan uplift prior to the Eocene–Oligocene climate transition: evidence from pollen analysis of the Xining Basin. Geology 36, 987–990.
Eren, M., 2011. Stable isotope geochemistry of Quaternary calcretes in the Mersin area, southern Turkey—a comparison and implications for their origin. Chem. Erde 71, 31–37.
Fan, M.J., DeCelles, P.G., Gehrels, G.E., Dettman, D.L., Quade, J., Peyton, S.L., 2011. Sedimentology, detrital zircon geochronology, and stable isotope geochemistry of the lower Eocene strata in the Wind River Basin, central Wyoming. Geol. Soc. Am. Bull. 123, 979–996.
Fang, X.M., Garzione, C., Van der Voo, R., Li, J.J., Fan, M.J., 2003. Flexural subsidence by 29 Ma on the NE edge of Tibet from the magnetostratigraphy of Linxia Basin, China. Earth Planet. Sci. Lett. 210, 545–560.
Fang, X.M., Zhang, W.L., Meng, Q.Q., Gao, J.P., Wang, X.M., King, J., Song, C.H., Dai, S., Miao, Y.F., 2007. High-resolution magnetostratigraphy of the Neogene Huaitoutala section in the eastern Qaidam Basin on the NE Tibetan Plateau, Qinghai Province, China and its implication on tectonic uplift of the NE Tibetan Plateau. Earth Planet. Sci. Lett. 258, 293–306.
Fang, Q., Hong, H., Zhao, L., Furnes, H., Lu, H., Han, W., Liu, Y., Jia, Z., Wang, C., Yin, K., Algeo, T.J., 2017. Tectonic uplift-influenced monsoonal changes promoted hominin occupation of the Luonan Basin: insights from a loess-paleosol sequence, eastern Qinling Mountains, central China. Quat. Sci. Rev. 169, 312–329.
Fontes, J.C., Gasse, F., Gibert, E., 1996. Holocene environmental changes in Lake Bangong basin (Western Tibet). Part 1: chronology and stable isotopes of carbonates of a Holocene lacustrine core. Palaeogeogr. Palaeoclimatol. Palaeoecol. 120, 25–47.
Gallagher, T.M., Sheldon, N.D., 2016. Combining soil water balance and clumped isotopes to understand the nature and timing of pedogenic carbonate formation. Chem. Geol. 435, 79–91.
Gradstein, F.M., Ogg, J.G., Schmitz, M.D., Ogg, G.M., 2012. The Geological Time Scale 2012. Vol. 2 Elsevier, Waltham, Massachusetts (708 pp).
Hoke, G.D., Liu-Zeng, J., Hren, M.T., Wissink, G.K., Garzione, C.N., 2014. Stable isotopes reveal high southeast Tibetan Plateau margin since the Paleogene. Earth Planet. Sci. Lett. 394, 270–278.
Hollis, C.J., Handley, L., Crouch, E.M., Morgans, H.E.G., Baker, J.A., Creech, J., Collins, K.S., Gibbs, S.J., Huber, M., Schouten, S., Zachos, J.C., Pancost, R.D., 2009. Tropical sea temperatures in the high latitude South Pacific during the Eocene. Geology 37 (2), 99–102.
Hollis, C.J., Taylor, K.W., Handley, L., Pancost, R.D., Huber, M., Creech, J.B., Hines, B.R., Crouch, E.M., Morgans, H.G., Crampton, G.S., Pearson, P.N., Zachos, J.C., 2012. Early Paleogene temperature history of the Southwest Pacific Ocean: reconciling proxies and models. Earth Planet. Sci. Lett. 349, 53–66.
Hong, H.L., Li, Z.H., Xue, H.J., Zhu, Y.H., Zhang, K.X., Xiang, S.Y., 2007. Oligocene clay mineralogy of the Linxia basin: evidence of paleoclimatic evolution subsequent to the initial-stage uplift of the Tibetan Plateau. Clay Clay Miner. 55, 492–505.
Hong, H.L., Zhang, K.X., Li, Z.H., 2010a. Climatic and tectonic uplift evolution since 7 Ma in Gyirong basin, southwestern Tibet Plateau: clay mineral evidence. Int. J. Earth Sci. 99, 1305–1315.
Hong, H.L., Wang, C.W., Xu, Y.D., Zhang, K.X., Yin, K., 2010b. Paleoclimate evolution of the Qinghai-Tibet Plateau since the Cenozoic. Earth Sci. J. China Univ. Geosci. 35 (5), 728–736 (in Chinese with English abstract).
Hong, H.L., Fang, Q., Cheng, L., Wang, C.W., Churchman, G.J., 2016. Microorganism induced weathering of clay minerals in a hydromorphic soil. Geochim. Cosmochim. Acta 184, 272–288.
Horiuchi, Y., Hisada, K., Lee, Y.I., 2009. Paleosol horizons in the Shiohama Formation of the Lower Cretaceous Kanmon Group, Southwest Japan and implications for sediment supply frequency. Cretac. Res. 30 (5), 1313–1324.
Hough, B.G., Garzione, C.N., Wang, Z., Lease, R.O., Burbank, D.W., Yuan, D.Y., 2011. Stable isotope evidence for topographic growth and basin segmentation: implications for the evolution of the NE Tibetan Plateau. Geol. Soc. Am. Bull. 123, 168–185.
Hough, B.G., Fan, M.J., Passey, B.H., 2014. Calibration of the clumped isotope geothermometer in soil carbonate in Wyoming and Nebraska, USA: implications for paleoelevation and paleoclimate reconstruction. Earth Planet. Sci. Lett. 391, 110–120.
Huang, H.C., Huang, Q.H., Ma, S., 1996. Geology of Qaidam Basin and Its Petroleum Prediction. Geological Publishing House, Beijing (257 pp, in Chinese).
Huntington, K.W., Saylor, J., Quade, J., Hudson, A.M., 2015. High late Miocene–Pliocene elevation of the Zhada Basin, southwestern Tibetan Plateau, from carbonate clumped isotope thermometry. Geol. Soc. Am. Bull. 127, 181–199.
Hyland, E., Sheldon, N.D., Fan, M.J., 2013. Terrestrial paleoenvironmental reconstructions indicate transient peak warming during the early Eocene climatic optimum. Geol. Soc. Am. Bull. 125 (7–8), 1338–1348.
IAEA & WMO, 2012. Global Network of Isotopes in Precipitation. (Available at: www-naweb.iaea. org/napc/ih/index.html, accessed: April 26th, 2016).
Jackson, M.L., 1985. Soil Chemical Analysis Advanced Course, 2nd ed. (Madison, Wisconsin, 895 pp).
Ji, J.L., Zhang, K.X., Clift, P.D., Zhuang, G.S., Song, B.W., Ke, X., Xu, Y.D., 2017. High-resolution magnetostratigraphic study of the Paleogene-Neogene strata in the Northern Qaidam Basin: implications for the growth of the Northeastern Tibetan Plateau. Gondwana Res. 46, 141–155.
Jian, X., Guan, P., Zhang, D.W., Zhang, W., Feng, F., Liu, R.J., Lin, S.D., 2013. Provenance of Tertiary sandstone in the northern Qaidam basin, northeastern Tibetan Plateau: integration of framework petrography, heavy mineral analysis and mineral chemistry. Sediment. Geol. 290, 109–125.
Jian, X., Guan, P., Fu, S.T., Zhang, D.W., Zhang, W., Zhang, Y.S., 2014. Miocene sedimentary environment and climate change in the northwestern Qaidam basin, northeastern Tibetan Plateau: facies, biomarker and stable isotopic evidences. Palaeogeogr. Palaeoclimatol. Palaeoecol. 414, 320–331.
Kahle, M., Kleber, M., Jahn, R., 2002. Review of XRD-based quantitative analyses of clay minerals in soils: the suitability of mineral intensity factors. Geoderma 109 (3), 191–205.
Ke, X., Ji, J.L., Zhang, K.X., Kou, X.H., Song, B.W., Wang, C.W., 2013. Magnetostratigraphy and anisotropy of magnetic susceptibility of the Lulehe Formation in the northeastern Qaidam Basin. Acta Geol. Sin. (Engl. Ed.) 87 (2), 576–587.
Kent-Corson, M.L., Ritts, B.D., Zhuang, G.S., Bovet, P.M., Graham, S.A., Chamberlain, P.C., 2009. Stable isotopic constraints on the tectonic, topographic, and climatic evolution of the northern margin of the Tibetan Plateau. Earth Planet. Sci. Lett. 282, 158–166.
Kim, S.-T., O'Neil, J.R., 1997. Equilibrium and nonequilibrium oxygen isotope effects in synthetic carbonates. Geochim. Cosmochim. Acta 61, 3461–3475.
Koch, P.L., 1998. Isotopic reconstruction of past continental environments. Annu. Rev. Earth Planet. Sci. 26, 573–613.
Kraus, M.J., 1996. Alluvial deposits in lower Eocene alluvial rocks, Bighorn Basin, Wyoming. J. Sediment. Res. 66, 354–363.
Kraus, M.J., 1997. Lower Eocene alluvial paleosols: pedogenic development, stratigraphic relationships, and paleosol/landscape associations. Palaeogeogr. Palaeoclimatol. Palaeoecol. 129 (3), 387–406.
Kubler, B., 1997. Concomitant alteration of clay minerals and organic matter during burial diagenesis. In: Paquet, H., Clauer, N. (Eds.), Soil and Sediments: Mineralogy and Geochemistry. Springer, Berlin, pp. 327–362.
Lallier, F., Antoine, C., Charreau, J., Caumon, G., Ruiu, J., 2013. Management of ambiguities in magnetostratigraphic correlation. Earth Planet. Sci. Lett. 371, 26–36.
Leier, J., Quade, J., DeCelles, P., Kapp, P., 2009. Stable isotopic results from paleosol carbonate in South Asia: paleoenvironmental reconstructions and selective alteration. Earth Planet. Sci. Lett. 279, 242–254.
Li, L.L., Garzione, C.N., 2017. Spatial distribution and controlling factors of stable isotopes in meteoric waters on the Tibetan Plateau: implications for paleoelevation reconstruction. Earth Planet. Sci. Lett. 460, 302–314.
Li, L., Garzione, C.N., Pullen, A., Chang, H., 2016. Early-middle Miocene topographic growth of the northern Tibetan Plateau: stable isotope and sedimentation evidence from the southwestern Qaidam basin. Palaeogeogr. Palaeoclimatol. Palaeoecol. 461, 201–213.
Li, L.L., Wu, C.D., Fang, F.F., Li, J.J., Zhang, C.H., 2017. Carbon and oxygen isotopic constraints on paleoclimate and paleoelevation of the southwestern Qaidam basin, northern Tibetan Plateau. Geosci. Front. 8 (5), 1175–1186.
Lister, G.S., Kelts, K., Zao, C.K., Yu, J.Q., Niessen, F., 1991. Lake Qinghai, China: closed-basin like levels and the oxygen isotope record for ostracoda since the latest Pleistocene. Palaeogeogr. Palaeoclimatol. Palaeoecol. 84, 141–162.
Liu, Z.C., Wang, Y.J., Chen, Y., Li, X.S., Li, Q.C., 1998. Magnetostratigraphy and sedimentologically derived geochronology of the Quaternary lacustrine deposits of a 3000 m thick sequence in the central Qaidam Basin, western China. Palaeogeogr. Palaeoclimatol. Palaeoecol. 140, 459–473.
Liu, Y.D., Gan, Y.Q., Yu, T.T., Liu, C.F., Zhou, A.G., 2010. Online simultaneous determination of δD and $\delta^{18}O$ in microliter water samples by thermal conversion/elemental analysis isotope ratio mass spectrometry. Rock Miner. Anal. 29, 643–647 (in Chinese with English abstract).
Liu, Z.H., Zhang, K.X., Sun, Y.Y., Liu, W.G., Liu, Y.S., Quan, C., 2014. Cenozoic environmental changes in the northern Qaidam Basin inferred from n-alkane records. Acta Geol. Sin. (Engl. Ed.) 88 (5), 1547–1555.
Lowenstein, T.K., Demicco, R.V., 2006. Elevated Eocene atmospheric CO_2 and its subsequent decline. Science 303, 1928.
Lu, H.J., Xiong, S.F., 2009. Magnetostratigraphy of the Dahonggou section, northern Qaidam Basin and its bearing on Cenozoic tectonic evolution of the Qilian Shan and Altyn Tagh Fault. Earth Planet. Sci. Lett. 288, 539–550.
Lu, J.F., Song, B.W., Chen, R.M., Zhang, J.Y., Ye, H., 2010. Palynological assemblage of Eocene-Oligocene pollen and their biostratigraphic correlation in Dahonggou, Daqaidam Regions, Qaidam Basin. Earth Sci. J. China Univ. Geosci. (Wuhan) 35 (5), 839–848 (in Chinese with English abstract).
Lu, H.J., Fu, B.H., Shi, P.L., Ma, Y.X., Li, H.B., 2016. Constraints on the uplift mechanism of northern Tibet. Earth Planet. Sci. Lett. 453, 108–118.
Mack, G.H., James, W.C., Monger, H.C., 1993. Classification of paleosols. Geol. Soc. Am. Bull. 105, 129–136.
McCarthy, P.J., Martini, I.P., Leckie, D.A., 1997. Anatomy and evolution of a Lower Cretaceous alluvial plain: sedimentology and paleosols in the upper Blairmore Group, southwestern Alberta, Canada. Sedimentology 44, 197–220.
McCarthy, P.J., Martini, I.P., Leckie, D.A., 1998. Use of micromorphology for interpretation of complex alluvial paleosols: examples from the Mill Creek Formation (Albian), southwestern Alberta, Canada. Palaeogeogr. Palaeoclimatol. Palaeoecol.

143, 87–110.
Metivier, F., Gaudemer, Y., Tapponnier, P., Meyer, B., 1998. Northeastward growth of the Tibet Plateau deduced from balanced reconstruction of two depositional areas: the Qaidam and Hexi Corridor basins, China. Tectonics 17, 823–842.
Meyer, N.A., Breecker, D.O., Young, M.H., Litvak, M.E., 2014. Simulating the effect of vegetation in formation of pedogenic carbonate. Soil Sci. Soc. Am. J. 78 (3), 914–924.
Miall, A.D., 1977. A review of the braided river depositional environments. Earth Sci. Rev. 13, 1–62.
Miall, A.D., 1996. The Geology of Fluvial Deposits. Springer, Heidelberg (582 pp).
Miao, Y.F., Fang, X.M., Herrmann, M., Wu, F.L., Zhang, Y., Liu, D.L., 2011. Miocene pollen record of KC-1 core in the Qaidam Basin, NE Tibetan Plateau and implications for evolution of the East Asian monsoon. Palaeogeogr. Palaeoclimatol. Palaeoecol. 209, 30–38.
Miao, Y.F., Wu, F.L., Chang, H., Fang, X.M., Deng, T., Sun, J.M., Jin, C.S., 2016. A Late-Eocene palynological record from the Hoh Xil Basin, northern Tibetan Plateau, and its implications for stratigraphic age, paleoclimate and paleoelevation. Gondwana Res. 31, 241–252.
Miller, K.G., Fairbanks, R.G., Mountain, G.S., 1987. Tertiary oxygen isotope synthesis, sea level history, and continental margin erosion. Paleoceanography 2, 1–19.
Moore, D.M., Reynolds, R.C., 1989. X-ray Diffraction and the Identification and Analysis of Clay Minerals. Oxford University Press, Oxford (332 pp).
Nemec, W., Steel, R.J., 1988. Fan Deltas: Sedimentology and Tectonic Settings. Blackie (444 pp).
Nesbitt, H.W., Young, G.M., 1984. Prediction of some weathering trends of plutonic and volcanic rocks based on thermodynamic and kinetic considerations. Geochim. Cosmochim. Acta 48, 1523–1534.
Passey, B.H., Levin, N.E., Cerling, T.E., Brown, F.H., Eiler, J.M., 2010. High-temperature environments of human evolution in East Africa based on bond ordering in paleosol carbonates. Proc. Natl. Acad. Sci. U.S.A. 107 (25), 245–249.
Pearson, P.N., van Dongen, B.E., Nicholas, C.J., Pancost, R.D., Schouten, S., Singano, J.M., Wade, B.S., 2007. Stable warm tropical climate through the Eocene Epoch. Geology 35, 211–214.
Peters, N.A., Huntington, K.W., Hoke, G.D., 2013. Hot or not? Impact of seasonally variable soil carbonate formation on paleotemperature and O-isotope records from clumped isotope thermometry. Earth Planet. Sci. Lett. 361, 208–218.
Pollastro, R.M., 1993. Considerations and applications of the illite/smectite geothermometer in hydrocarbon-bearing rocks of Miocene to Mississippian age. Clay Clay Miner. 41, 119–133.
QBGMR (Qinghai Bureau of Geology and Mineral Resources), 1991. Regional Geology of the Qinghai Province. Geological Publishing House, Beijing, pp. 604 in Chinese).
Quade, J., Cerling, T.E., Bowman, J.R., 1989. Systematic variations in the stable carbon and oxygen isotopic composition of pedogenic carbonate along elevation transects in the southern Great Basin, United States. Geol. Soc. Am. Bull. 101, 464–475.
Quade, J., Garzione, C., Eiler, J., 2007. Paleoelevation reconstruction using pedogenic carbonates. Rev. Mineral. Geochem. 66 (1), 53–87.
Quade, J., Breecker, D.O., Daeron, M., Eiler, J., 2011. The paleoaltimetry of Tibet: an isotopic perspective. Am. J. Sci. 311, 77–115.
Quade, J., Eiler, J., Daeron, M., Achyuthan, H., 2013. The clumped isotope geothermometer in soil and paleosol carbonate. Geochim. Cosmochim. Acta 105, 92–107.
Retallack, G.J., 2001a. Soils of the Past, 2nd ed. Unwin Hyman, London, pp. 520.
Retallack, G.J., 2001b. A 300-million-year record of atmospheric carbon dioxide from fossil plant cuticles. Nature 411, 287–290.
Retallack, G.J., 2005. Pedogenic carbonate proxies of amount and seasonality of precipitation. Geology 33, 333–336.
Retallack, G.J., 2007. Cenozoic paleoclimate on land in North America. J. Geol. 115, 271–294.
Reynolds Jr., R.C., 1985. NEWMOD: A Computer Program for the Calculation of One-dimensional Diffraction Patterns for Mixed-layered Clays. RC Reynolds, 8 Brook Rd, Hanover, New Hampshire.
Rieser, A.B., Neubauer, F., Liu, Y., Ge, X., 2005. Sandstone provenance of north-western sectors of the intracontinental Cenozoic Qaidam Basin, western China: tectonic vs. climatic control. Sediment. Geol. 177, 1–18.
Rieser, A.B., Liu, Y.J., Genser, J., Neubauer, F., Handler, R., Ge, X.H., 2006. Uniform Permian $^{40}Ar/^{39}Ar$ detrital mica ages in the eastern Qaidam Basin (NW China): where is the source? Terra Nova 18, 79–87.
Rowley, D.B., Garzione, C.N., 2007. Stable isotope-based paleoaltimetry. Annu. Rev. Earth Planet. Sci. 35, 463–508.
Rozanski, K., Araguas-Araguas, L., Gonfiantini, R., 1993. Isotopic patterns in modern global precipitation. In: Swart, P.K., Lohmann, K.C., McKenzie, J., Savin, S. (Eds.), Climate Change in Continental Isotopic Records. American Geophysical Union, Washington, D.C., pp. 36.
Setti, M., Lópezgalindo, A., Padoan, M., Garzanti, E., 2014. Clay mineralogy in southern Africa river muds. Clay Miner. 49 (5), 717–733.
Shackleton, N., Boersma, A., 1981. The climate of the Eocene ocean. J. Geol. Soc. Lond. 138, 153–157.
Sheldon, N.D., Tabor, N.J., 2009. Quantitative and paleoenvironmental and paleoclimatic reconstruction using paleosols. Earth Sci. Rev. 95, 1–52.
Sheldon, N.D., Retallack, G.J., Tanaka, S., 2002. Geochemical climofunctions from North American soils and applications to paleosols across the Eocene–Oligocene boundary in Oregon. J. Geol. 110, 687–696.
Shellito, C.J., Sloan, L.C., Huber, M., 2003. Climate model sensitivity to atmospheric CO_2 levels in early-middle Paleogene. Palaeogeogr. Palaeoclimatol. Palaeoecol. 193, 113–123.
Singer, A., 1984. The palaeoclimatic interpretation of clay minerals in sediments – a review. Earth Sci. Rev. 21, 251–293.
Singh, S., Parkash, B., Awasthi, A.K., Singh, T., 2012. Palaeoprecipitation record using O-isotope studies of the Himalayan Foreland Basin sediments, NW India Seema. Palaeogeogr. Palaeoclimatol. Palaeoecol. 331–332, 39–49.
Smith, R.Y., Greenwood, D.R., Basinger, J.F., 2010. Estimating paleoatmospheric pCO_2 during the EECO from stomatal frequency of Ginkgo, Okanagan Highlands, British Columbia, Canada. Palaeogeogr. Palaeoclimatol. Palaeoecol. 293, 120–131.
Snell, K.E., Thrasher, B.L., Eiler, J.M., Koch, P.L., Sloan, L.C., Tabor, N.J., 2013. Hot summers in the Bighorn Basin during the early Paleogene. Geology 41, 55–58.
Song, X.Y., Spicer, R.A., Yang, J., Yao, Y.F., Li, C.S., 2010. Pollen evidence for an Eocene to Miocene elevation of central southern Tibet predating the rise of the High Himalaya. Palaeogeogr. Palaeoclimatol. Palaeoecol. 297 (1), 159–168.
Song, B.W., Zhang, K.X., Lu, J.F., Wang, C.W., Xu, Y.D., 2013. The middle Eocene to early Miocene integrated sedimentary record in the Qaidam Basin and its implications for paleoclimate and early Tibetan Plateau uplift. Can. J. Earth Sci. 50 (2), 183–196.
Song, C.H., Hu, S.H., Han, W.X., Zhang, T., Fang, X.M., Gao, J.P., Wu, F.L., 2014. Middle Miocene to earliest Pliocene sedimentological and geochemical records of climate change in the western Qaidam Basin on the NE Tibetan Plateau. Palaeogeogr. Palaeoclimatol. Palaeoecol. 395, 67–76.
Song, B.W., Ji, J.L., Wang, C.W., Xu, Y.D., Zhang, K.X., 2017. Intensified aridity in the Qaidam Basin during the middle Miocene: constraints from ostracod, stable isotope and weathering records. Can. J. Earth Sci. 54 (3), 242–256.
Strömberg, C.A.E., 2011. Evolution of grasses and grassland ecosystems. Annu. Rev. Earth Planet. Sci. 39, 517–544.
Sun, Y.Y., 2014. Cenozoic Climatic and Environmental Changes in the Qaidam Basin (Unpubl. Thesis). University of Hong Kong, Pokfulam, Hong Kong SAR. http://dx.doi.org/10.5353/th_b5223961.
Sun, Z.C., Feng, X.J., Li, D.M., Yang, F., Qu, Y.H., Wang, H.J., 1999. Cenozoic Ostracoda and palaeoenvironments of the northeastern Tarim Basin, western China. Palaeogeogr. Palaeoclimatol. Palaeoecol. 148, 37–50.
Sun, Z.M., Yang, Z.Y., Pei, J.L., Ge, X.H., Wang, X.S., Yang, T.S., Li, W.M., Yuan, S.H., 2005. Magnetostratigraphy of Paleogene sediments from northern Qaidam Basin, China: implications for tectonic uplift and block rotation in northern Tibetan Plateau. Earth Planet. Sci. Lett. 237, 635–646.
Sun, J.M., Xu, Q.H., Liu, W.M., Zhang, Z.Q., Xue, L., Zhao, P., 2014. Palynological evidence for the latest Oligocene-early Miocene paleoelevation estimate in the Lunpola Basin, central Tibet. Palaeogeogr. Palaeoclimatol. Palaeoecol. 399, 21–30.
Thrasher, B.L., Sloan, L.C., 2009. Carbon dioxide and the early Eocene climate of western North America. Geology 37, 807–810.
Tipple, B.J., Meyers, S.R., Pagani, M., 2010. Carbon isotope ratio of Cenozoic CO_2: a comparative evaluation of available geochemical proxies. Paleoceanography 25, PA3202.
Veizer, J., Ala, D., Azmy, K., Bruckschen, P., Buhl, D., Bruhn, F., Carden, G.A.F., Diener, A., Ebneth, S., Godderis, Y., Jasper, T., Korte, C., Pawellek, F., Podlaha, O.G., Strauss, H., 1999. $^{87}Sr/^{86}Sr$, $\delta^{13}C$ and $\delta^{18}O$ evolution of Phanerozoic seawater. Chem. Geol. 161, 59–88.
Wanas, H.A., Sallam, E., Zobaa, M.K., Li, X., 2015. Mid-Eocene alluvial-lacustrine succession at Gebel El-Goza El-Hamra (Shabrawet area, NE Eastern Desert, Egypt): facies analysis, sequence stratigraphy and paleoclimatic implications. Sediment. Geol. 329, 115–129.
Wang, J.H., 2006. Paleomagnetism and Kinematics Study on the Cenozoic Qaidam Basin (Masters Thesis). Northwest University, Xian, China (53 pp).
Wang, J., Wang, Y.J., Liu, Z.C., Li, J.Q., Xi, P., 1999. Cenozoic environmental evolution of the Qaidam Basin and its implications for the uplift of the Tibetan Plateau and the drying of central Asia. Palaeogeogr. Palaeoclimatol. Palaeoecol. 152 (1), 37–47.
Wang, X.M., Qiu, Z.D., Li, Q., Wang, B.Y., Qiu, Z.X., Downs, W.R., Xie, G.P., Xie, J.Y., Deng, T., Takeuchi, G.T., Tseng, Z.J., Chang, M.M., Liu, J., Wang, Y., Biasatti, D., Sun, Z.C., Fang, X.M., Meng, Q.Q., 2007. Vertebrate paleontology, biostratigraphy, geochronology, and paleoenvironment of Qaidam Basin in northern Tibetan Plateau. Palaeogeogr. Palaeoclimatol. Palaeoecol. 254, 363–385.
Wang, Y., Deng, T., Flynn, L., Wang, X.F., Yin, A., Xu, Y.F., Parker, W., Lochner, E., Zhang, C.F., Biasatti, D., 2012. Late Neogene environmental changes in the central Himalaya related to tectonic uplift and orbital forcing. J. Asian Earth Sci. 44, 62–76.
Wang, C.W., Adriaens, R., Hong, H.L., Elsen, J., Vandenberghe, N., Lourens, L.J., Gingerich, P.D., Abels, H.A., 2017. Clay mineralogical constraints on weathering in response to early Eocene hyperthermal events in the Bighorn Basin, Wyoming (Western Interior, USA). Geol. Soc. Am. Bull. B31515, 1.
Wang, W.T., Zheng, W.J., Zhang, P.Z., Li, Q., Kirby, E., Yuan, D.Y., Zheng, D.W., Liu, C.C., Wang, Z.C., Zhang, H.P., Pang, J.Z., 2017. Expansion of the Tibetan plateau during the Neogene. Nat. Commun. 8, 15887.
Wilson, M.D., Pittman, E.D., 1977. Authigenic clays in sandstones; recognition and influence on reservoir properties and paleoenvironmental analysis. J. Sediment. Res. 47, 3–31.
Wu, H.C., Zhang, S.H., Han, Y.G., 2002. The terranes motion in western China: paleomagnetic evidence and their problems. Earth Sci. Front. 9 (4), 355–369.
Xia, W.C., Zhang, N., Yuan, X.P., Fan, L.S., Zhang, B.S., 2001. Cenozoic Qaidam basin, China: a stronger tectonic inversed, extensional rifted basin. Am. Assoc. Pet. Geol. Bull. 85, 715–736.
Xiao, G.Q., Abels, H.A., Yao, Z.Q., Dupont-Nivet, G., Hilgen, F.J., 2010. Asian aridification linked to the first step of the Eocene–Oligocene climate Transition (EOT) in obliquity-dominated terrestrial records (Xining Basin, China). Clim. Past 6, 501–513.
Xiao, X., Horton, R., Sauer, T., Heitman, J., Ren, T., 2011. Cumulative soil water evaporation as a function of depth and time. Vadose Zone J. 10, 1016–1022.
Yang, P., 2000. Ostracods extinction and explosion events of the Mesozoic-Cenozoic in Qaidam basin, North China. J. Palaeogeogr. 2 (3), 69–74 (in Chinese with English abstract).
Yang, F., Ma, Z.Q., Xu, T.C., Ye, S.J., 1992. A tertiary paleomagnetic stratigraphic profile in Qaidam basin. Acta Petrol. Sin. 13, 97–101 (in Chinese with English Abstract).

Yang, F., Qiao, Z.Z., Zhang, H.Q., Zhang, Y.H., Sun, Z.C., 2006. Features of the Cenozoic ostracod fauna and environmental significance in Qaidam Basin. J. Palaeogeogr. 8, 143–156 (in Chinese with English abstract).

Yao, T.D., Masson-Delmotte, V., Gao, J., Yu, W.S., Yang, X.Y., Risi, C., Sturm, C., Werner, M., Zhao, H.B., He, Y., Ren, W., Tian, L.D., Shi, C.M., Hou, S.G., 2013. A review of climatic controls on $\delta^{18}O$ in precipitation over the Tibetan Plateau: observations and simulations. Rev. Geophys. 51, 525–548.

Yapp, C.J., 2004. Fe(CO3)OH in goethite from a mid-latitude North American oxisol: estimate of atmospheric CO_2 concentration in the Early Eocene "climatic optimum". Geochim. Cosmochim. Acta 68, 935–947.

Zachos, J.C., Stott, L.D., Lohmann, K.C., 1994. Evolution of early Cenozoic marine temperatures. Paleoceanography 9, 353–387.

Zachos, J.C., Pagani, M., Sloan, L., Thomas, E., Billups, K., 2001. Trends, rhythms, and aberrations in global climate 65 Ma to present. Science 292, 686–693.

Zachos, J.C., Dickens, G.R., Zeebe, R.E., 2008. An early Cenozoic perspective on greenhouse warming and carbon-cycle dynamics. Nature 451, 279–283.

Zhang, W.L., 2006. Cenozoic Uplift of the Tibetan Plateau: Evidence From High Resolution Magnetostratigraphy of the Qaidam Basin (Ph.D. thesis). Lanzhou University, Lanzhou, China (245 pp).

Zhang, K.X., Wang, G.C., Cao, K., Liu, C., Xiang, S.Y., Hong, H.L., Kou, X.H., Xu, Y.D., Chen, F.M., Meng, Y.N., Chen, R.M., 2008. Cenozoic sedimentary records and geochronological constraints of differentia uplift of the Qinghai-Tibet plateau. Sci. China D Earth Sci. 51, 1658–1672.

Zhu, P.C., 2015. Groundwater Circulation Patterns of Yuqia-Mahai Basin in the Middle and Lower Reaches of Yuqia River (Masters Thesis). Jilin University, Jilin, China (48 pp).

Zhuang, G.S., Hourigan, J.K., Koch, P.L., Ritts, B.D., Kent-Corson, M.L., 2011a. Isotopic constraints on intensified aridity in Central Asia around 12 Ma. Earth Planet. Sci. Lett. 312 (1–2), 152–163.

Zhuang, G.S., Hourigan, J.K., Ritts, B.D., Kent-Corson, M.L., 2011b. Cenozoic multiple-phase tectonic evolution of the northern Tibetan Plateau: constraints from sedimentary records from Qaidam Basin, Hexi Corridor, and Subei Basin, northwest China. Am. J. Sci. 311, 116–152.

Zhuang, G.S., Brandon, M.T., Pagani, M., Krishnan, S., 2014. Leaf wax stable isotopes from Northern Tibetan Plateau: implications for uplift and climate since 15 Ma. Earth Planet. Sci. Lett. 390, 186–198.